East Asia orogenesis restricted oceanic circulation between Paleo-Tethys and Panthalassa before the Permian mass extinction

L. Zhao[1], H. Tang[1], R.N. Mitchell[1], Q.L. Li[1], X.W. Zhou[2], M.G. Zhai[1]

[1]State Key Laboratory of Lithospheric Evolution, Institute of Geology and Geophysics, Chinese Academy of Sciences, 100029, Beijing, China.

[2]Institute of Geology, Chinese Academy of Geological Sciences, 100037, Beijing, China.

Corresponding authors: L. Zhao (zhaolei@mail.iggcas.ac.cn), R.N. Mitchell (ross.mitchell@mail.iggcas.ac.cn), Q.L. Li (liqiuli@mail.iggcas.ac.cn), M.G. Zhai (mgzhai@mail.iggcas.ac.cn)

Key Points:

- Continental collision between the North and South China resulted in pervasive metamorphism in East Asia.
- New geochronological results reveal the onset of the collisional event during Permian, rather than Triassic as previously suggested.
- The orogenesis closed the seaway connecting Paleo-Tethys and Panthalassa before the Permian mass extinction.

Abstract

The Paleo-Tethys and Panthalassa are two major oceans that witnessed the end-Permian mass extinction, and they have been suggested to have distinct compositions, with the Paleo-Tethys Ocean euxinic, and the much larger Panthalassa Ocean being largely ventilated. Distinctions of these two once-connected oceans imply that interactions between them must have been restricted shortly before the end-Permian extinction. However, detailed geological processes for the disconnection between them along the eastern Paleo-Tethys Ocean due to the collision of North and South China, are still unclear. Previous geochronological studies on eclogite facies rocks in the Dabie–Sulu orogenic belt, which are the metamorphic products of the collision between North and South China, have yielded mainly Triassic metamorphic ages. Nonetheless, new Permian metamorphic ages are identified from southeastern North China, northern Dabie, and the Permo–Triassic intracontinental orogen of South China, which may collectively closely associate this major tectonic event with the end-Permian extinction. New age dating results, as well as a synthesis of recent studies on metamorphic rocks, show that the onset of the collisional orogenesis dates back to the Middle Permian (270–252 Ma). We thereby provide a new tectonic model for the major continents of East Asia, in which the initial collision between North and South China during the Middle Permian critically isolated the Paleo-Tethys Ocean from the Panthalassa Ocean, facilitating the oceanographic transition of the once fossiliferous Paleo-Tethys from a life-giving nutrient-rich ocean into a euxinic death trap, thereby serving as prelude to the end-Permian extinction.

Plain Language Summary

Earth's surface processes and environmental changes are strongly influenced by its deep geodynamics and the relations between the Siberian Traps and the end-Permian mass extinction is a good example. In addition to such a final trigger, the preconditioning of a vulnerable palaeoenvironment is being increasingly acknowledged as a critical aspect for understanding mass extinctions. In recent years, studies indicate that unlike the euxinic Paleo-Tethys Ocean, the much larger Panthalassa (a.k.a., paleo-Pacific) Ocean remained largely ventilated and provided potential refugia for marine taxa during the mass extinction. However, previous geochronological studies on eclogite facies rocks in the Dabie–Sulu orogenic belt, which are the metamorphic products of the collision between North and South China, have yielded mainly Triassic metamorphic ages postdating the Permian mass extinction. This study targeted the rocks from North China, northern Dabie orogen, and South China that escaped deep subduction. They all yield Permian metamorphic ages (270–252 Ma), which collectively indicate Permian continental collision between North and South China. This fundamental geological boundary condition would have critically isolated the Paleo-Tethys Ocean from the Panthalassa Ocean, and therefore, the poorly mixed Paleo-Tethys Ocean gradually became a dead sea, thereby preconditioning and facilitating the end-Permian biospheric crisis in the region.

1 Introduction

The biosphere experienced a devastating blow during the end-Permian, when more than 81% of marine species and ~89% of terrestrial species died out (Erwin et al., 2002; Fan et al., 2020; Viglietti et al., 2021). The Siberian Traps large igneous province has long been suggested to be the primary cause of the Permian mass extinction and related environmental stress (Burgess and

Bowring, 2015; Erwin, 1990). Additionally, other sources of volcanic outgassing around the world at that time, particularly the prolific magmatic arc of the Australian Tasmanides, also contributed to the overall volcanic-input aspect of the variegated kill mechanism (Chapman et al., 2022). Global oceanic anoxia and ocean acidification have also been proposed to have causal relations with the Permian extinction (Clarkson et al., 2015; Isozaki, 1997; Shen et al., 2011). However, global oceanic anoxia was challenged by several studies, which pointed out that the deep Panthalassa Ocean remained ventilated even during the expansion of the oxygen minimum zone (Algeo et al., 2011; Winguth and Winguth, 2012). Uncertainties also exist about the ability of the Siberian Traps and other sources of magmatism to have emitted enough toxic volatiles to sufficiently trigger the global climate and environmental changes, which in turn, resulted in the end-Permian mass extinction (Davydov and Karasev, 2021; Zhang et al., 2021b).

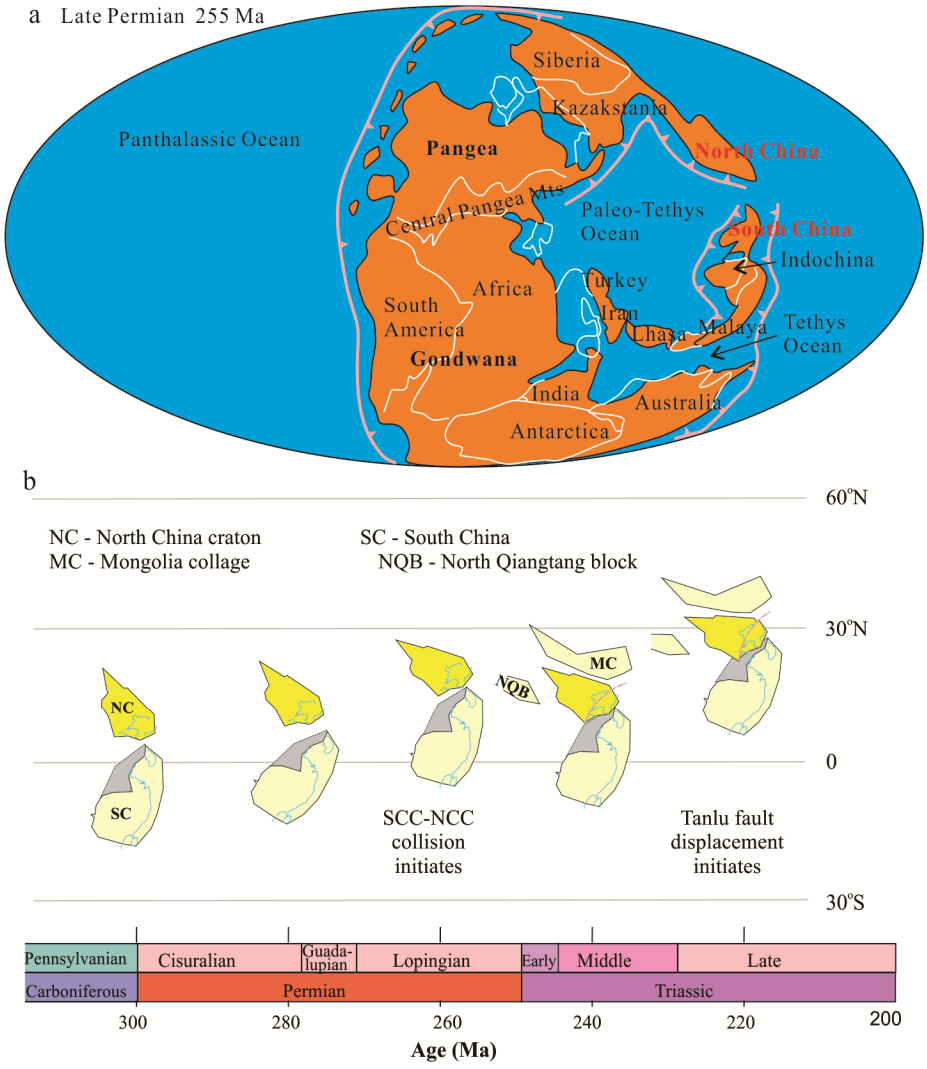

Fig. 1. Competing paleographic models of North and South China. (a) Early Triassic global paleogeography (Scotese, 1997). Note large gulf between North and South China. (b) Alterative interpretation of an earlier amalgamation of North and South China in the latest Permian (Huang et al., 2018).

Unlike the Panthalassa Ocean that occupied almost half of Earth's surface, the Paleo-Tethys Ocean was relatively small, comprising only 10–15% of the area of the global oceans, and was largely euxinic (Fig. 1a) (Algeo et al., 2008, 2011; Cao et al., 2009). Furthermore, almost all the type-localities of the stratigraphic sections preserving the paleontological record of the end-Permian extinction occur in the Paleo-Tethys tectonic realm (Şengör and Atayman, 2009), a feature which might be intrinsic to its euxinic condition. Previous studies reveal that the Paleo-Tethys Ocean was a nutrient trap that also exhibited features of a stagnant ocean while the Panthalassa Ocean underwent only limited redox changes and provided potential refugia for marine taxa that survived into the Triassic (Algeo et al., 2010; Algeo and Twitchett, 2010). The different features of the two late Paleozoic oceanic realms strongly suggest that oceanic circulation between them might have become severely restricted at some point (Şengör and Atayman, 2009). Due to the amalgamation of different continental blocks with Pangea before end-Permian, the Panthalassa and the Paleo-Tethys oceans were already disconnected along the northern, southern, and western margins of the Paleo-Tethys Ocean prior to the Middle Permian (Fig. 1a) (Carter et al., 2001; Metcalfe, 2006; Stampfli et al., 2013; Wu et al., 2020). Meanwhile, most paleogeographic models depict the eastern margin of the Paleo-Tethys Ocean as still being connected to the larger Panthalassa Ocean at the time of the extinction, and even well into the Triassic (Fig. 1a; Scotese, 1997). Therefore, the role that the eastern margin of the Paleo-Tethys Ocean played in oceanic circulation at this critical time is still unclear, mainly due to the ambiguous tectonic relationship between the North and South China cratons/blocks (hereafter referred to simply as North China and South China).

The final collision between these two continental blocks along the Dabie–Sulu orogenic belt resulted in the complete isolation of the Paleo-Tethys Ocean from the Panthalassa Ocean. However, constraining the timing of oceanic isolation is difficult because the dating of both orogenic metamorphism and magmatism tend to postdate the onset of continental collision (Roberts and Finger, 1997; Schmädicke et al., 2018). Currently, ages of eclogites from the Dabie–Sulu orogenic belt interpreted to reflect continental collision are Triassic (250–200 Ma; Jian et al., 2012; Liu et al., 2006; Zhou et al., 2011, 2015), which would appear to indicate that the isolation of the Paleo-Tethys Ocean from the Panthalassa Ocean occurred after the Permian mass extinction (Fig. 1a). These ages, however, are inconsistent with a paleogeographic reconstruction of East Asia derived from paleontological data that argue for the amalgamation of these two major continental blocks before the end-Permian, providing a united landmass for the Cathaysian biota and facilitating the formation of a stagnant Paleo-Tethys Ocean (Algeo et al., 2011; Cao and Zheng, 2009; Metcalfe, 1998, 2006; Yin et al., 2012, 2014). Although paleomagnetic data can place constraints on such an earlier initiation of this continental collision (Fig. 1b; Huang et al., 2018), their large uncertainties (~1,000 km) might preclude pinpointing the exact timing of when the Paleo-Tethys was cut off from the Panthalassa.

A potentially critically important clue for solving the Paleo-Tethys oceanic isolation problem that has been missing is an understanding of the significance of the initiation of the Permo–Triassic Sulu orogenic event of East Asia. This orogenic event not only resulted in the world-famous Dabie–Sulu ultrahigh pressure metamorphism, but also greatly influenced both North and South China, causing significant crustal thickening in southern North China (Li et al., 2017c; Liu et al., 2018), and an intracontinental orogenic belt in South China (Zhao et al., 2022). Unlike the ultrahigh pressure eclogites of the Sulu orogenic belt which are insensitive to initial continental collision, rocks of this region that did not experience deep subduction might be able

to better constrain the time of the initial collision. This study presents new geochronological results yielded using multiple dating techniques on low-grade metamorphic rocks in the northern Dabie orogenic belt and high-grade rocks from within South China. In addition, we also include a synthesis of recent studies of the Permo–Triassic metamorphism in southeastern North China, the Cathaysia block of southeastern South China, and the Dabie–Sulu orogenic belt.The initiation of the Permo–Triassic intracontinental orogeny as well as the timing of low-grade metamorphism in the northern Dabie orogenic belt consistently support a new Permo–Triassic tectonic paleogeographic reconstruction model for East Asia, with direct implications for more definitively constraining the timing of oceanic isolation with respect to the Permian mass extinction.

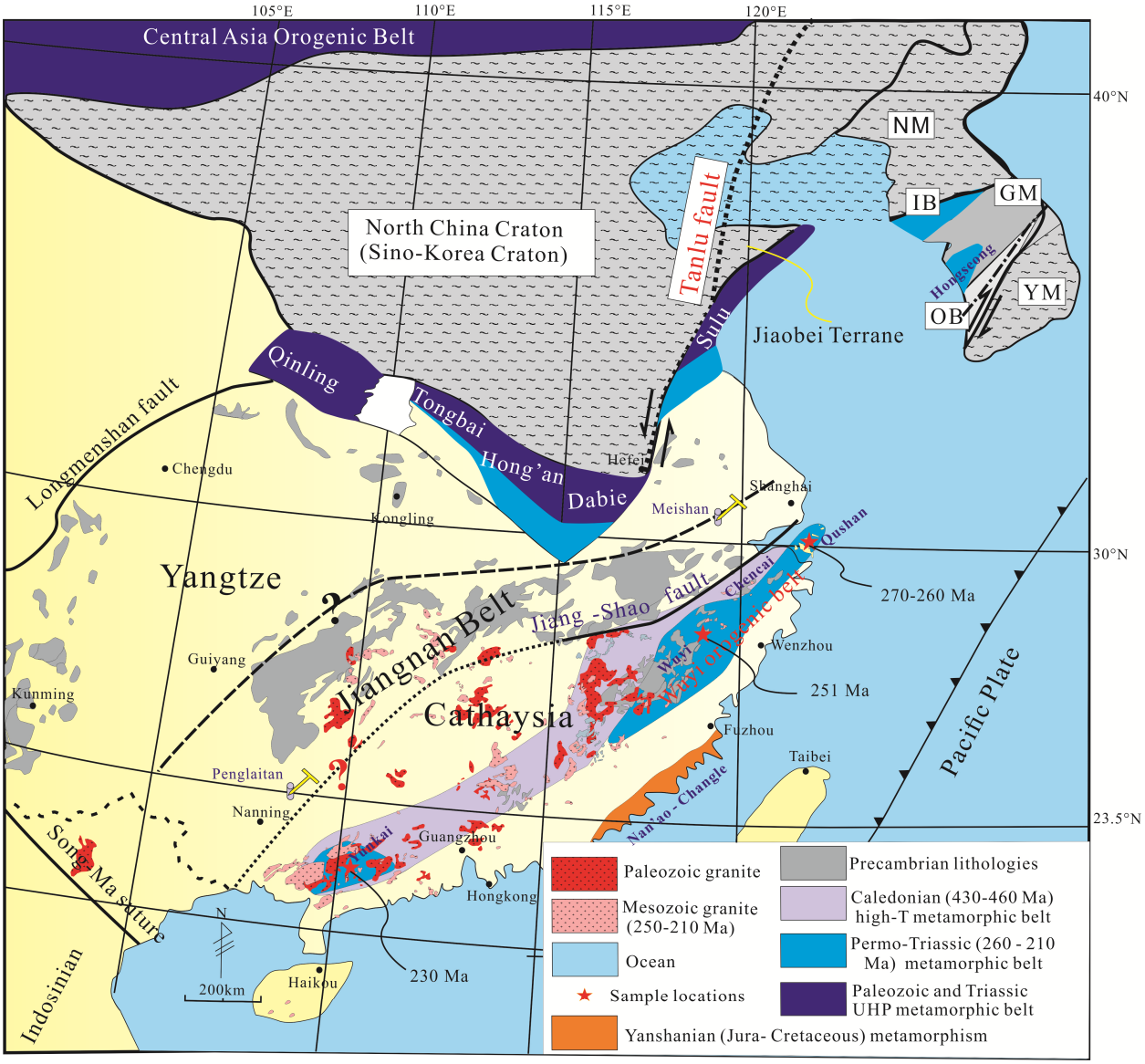

Fig. 2. Simplified geological map of East Eurasia. Modified after Zhao et al. (2015b, 2022).

2 Geological background and samples

East Asia is a composite of continental terranes including cratons/blocks of North China and South China. The North China craton (including the Korean Peninsula) is a continental block consisting of early Precambrian basement rocks tracing back to Eoarchean and experienced pervasive Neoarchean and Paleoproterozoic high-grade metamorphic reworkings (Wang et al., 2015; Zhai, 2011, 2014; Zhao, 2014). Its amalgamation with the South China and its subsequent decratonization are the most significant tectonic events witnessed by North China during the Phanerozoic (Wu et al., 2019; Yang et al., 2008; Zhu et al., 2012). The former tectonic event mainly affected rocks in southern and southeastern North China (along the Qinling–Dabie–Sulu orogenic belt; Fig. 2), which display Paleozoic–early Mesozoic high-pressure to ultra-high pressure metamorphism (An et al., 2018; Li et al., 2017c; Wang et al., 2014; Liu et al., 2021). Influence of the latter tectonic event is relatively more widespread, manifested by Mesozoic magmatism and thin-skinned deformation mainly in the central and eastern North China (Lin et al., 2011; Zhang et al., 2014b; Zhu et al., 2015).

South China was formed through the amalgamation of the Yangtze and the Cathaysia blocks during the Neoproterozoic, and is thought to have maintained its integrity ever since (Cawood et al., 2018, 2020; Li et al., 2009; Wang et al., 2013a). "Cathaysia" here has a different meaning from 'Cathaysialand' used in paleontological/ paleogeographic studies which refer to the much broader regions situated to the east of the Paleo-Tethys Ocean, including North China, South China, and Indochina (Metcalfe, 1998, 2006). The Yangtze block occupies the northwestern part of South China (Fig. 2), and has Archean and Paleoproterozoic basement components in its northern (Kongling) and southwestern (Cuoke near Kunming) marginal regions (Fig. 2) (Cui et al., 2021; Qiu et al., 2000; Wang et al., 2018; Ye et al., 2017; Zhang et al., 2006). Large areas of the Yangtze block remained stable during the Phanerozoic and tectonic events during the Paleozoic (South China Caledonian), and Mesozoic (Indosinian and Yanshanian) orogenic events affected mainly the marginal regions of this continental block (Faure et al., 2016; Li, 1994; Li and Li, 2007; Shu et al., 2008; Wang and Liou, 1991; Xiao and He, 2005). The famous Meishan and Penglaitan GSSP sections (Global Boundary Stratotype Section and Point) recording the end-Permian mass extinction occur in different parts of the Yangtze block (Fig. 2) (Cao and Zheng, 2009; Jin et al., 2000; Shen et al., 2019). The Cathaysia block is situated in the southeastern South China and is bounded by the Jiang–Shao fault with the rest of South China (Fig. 2). Early Precambrian lithologies have been discovered from different localities of this continental block (Shen et al., 2016; Xia and Xu, 2019; Zhang et al., 2021a; Zhao et al., 2015b). Metamorphism and related magmatism in the Paleozoic (also known as the South China Caledonian, 460–410 Ma), the Permo–Triassic (Indosinian), and the Late Mesozoic (Yanshanian) are each extensively developed in the Cathaysia block, and they exhibit a younging trend from northwest to southeast (Fig. 2). Both the Paleozoic and the Permo–Triassic tectonic events affected lower crustal components, as indicated by the occurrences of granulite facies rocks (Yu et al., 2003, 2005; Zhao et al., 2016, 2017, 2018), and they have both been suggested to be results of intracontinental orogens (Shu et al., 2014; Zhang et al., 2013a).

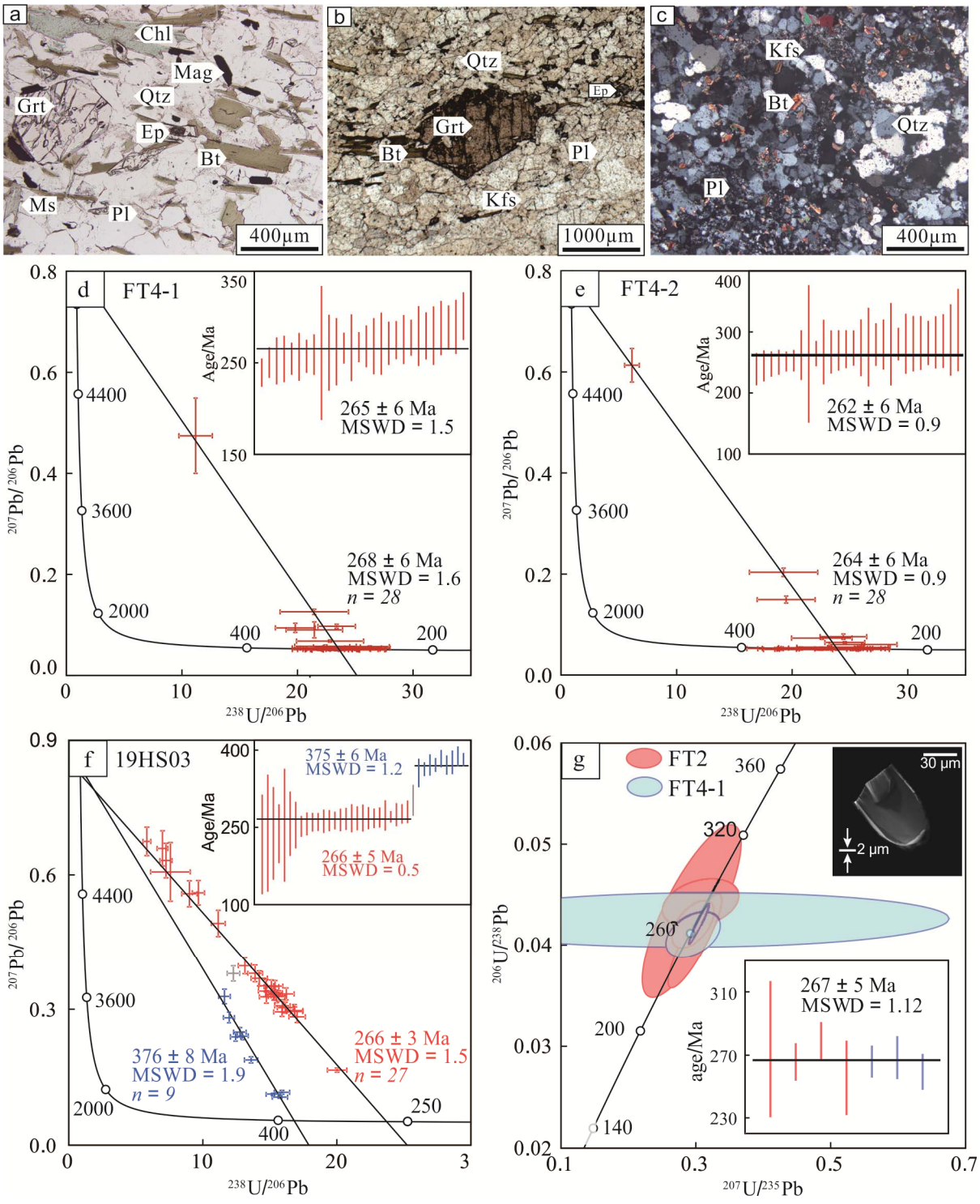

Fig. 3. Representative photomicrographs of the studied samples collected from the Beijiaiyang zone of northern Dabie orogen (a-c) and sating results (d-g) of the studied samples from the Beihuaiyang zone. (a) Garnet mica schist from the Foziling Group. (b) Garnet-bearing granitic gneiss. (c) Fine-grained biotite gneiss from the Luzhenguan Complex. (d-e) SIMS rutile U-Pb dating results of the two garnet mica schist samples from the Foziling Group. (f) SIMS titanite U-Pb dating results of the garnet-bearing granitic gneiss sample from the Luzhenguan Complex.

(g) SIMS U-Pb dating results of the unpolished zircon grains from one garnet mica schist sample (FT4-1) of the Foziling Group and one fine-grained biotite gneiss sample of the Luzhenguan Complex. Mineral abbreviations: Grt – garnet, Ms – muscovite, Pl – plagioclase, Bt – biotite, Qtz – quartz, Chl – chlorite, Ep – epidote, Kfs – K-feldspar, Mag – magnetite.

Southeast Asia, which is also in the Paleo-Tethys tectonic realm, consists two major continental terranes, the Indochina and the Sibumasu terranes. These two terranes have been suggested to have successively rifted off the northern margin of Gondwana during the Devonian and late Early Permian, respectively, and finally united during the Permo–Triassic (Metcalfe, 2006). There were several seaways connecting the Paleo-Tethys Ocean and the Panthalassa Ocean during the Permian, with the southern connection being the branch of the Paleo-Tethys between Indochina and South China, and the northern connection being the branch between North and South China (Fig. 1a). Intense controversies exist about both the timing and mechanism of the amalgamation of South China and Indochina which disconnected the Paleo-Tethys and the Panthalassa oceans in the south (Cocks and Torsvik, 2013; Faure et al., 2016; Lepvrier et al., 2004; Metcalfe, 1998, 2006). Different studies suggested subduction polarity along the Song Ma suture of both northward and southward during the consumption of a southern branch of the Paleo-Tethys Ocean prior to the amalgamation of these two continental blocks, with proposed final collisional ages ranging widely from prior to Late Silurian (Carter and Clift, 2008), Early Carboniferous (Metcalfe, 2006, 2013), and Triassic (Cocks and Torsvik, 2013; Faure et al., 2014, 2016; Zhang et al., 2014a). High-grade metamorphic rocks as well as strong deformation occurring along the Song Ma suture, and also in Vietnam, have been suggested to be products of the Indosinian orogeny in the Indochina Peninsula (Cocks and Torsvik, 2013; Faure et al., 2014, 2016; Nam et al., 2001; Roger et al., 2007; Zhang et al., 2014a). These metamorphic studies give undeniable evidence for Triassic metamorphic ages and have been widely employed to argue for Triassic collisional events between South China and Indochina (Nam et al., 2001; Roger et al., 2007; Zhang et al., 2013b). However, the geological significance of these high-grade metamorphic rocks is not unequivocal. As pointed out by Carter and Clift (2008), the Indosinian orogeny in Southeast Asia is not a Triassic mountain building event, but rather, is a tectonothermal reactivation event related to the accretion of the Sibumasu block to the Indochina block. Furthermore, palaeontological studies indicate that the distinctive Early Permian "Cathaysian" flora (*Gigantopteris*) is found in both South China and Indochina (Metcalfe, 2006), suggesting an early amalgamation of these two continental blocks prior to that time.

The northern seaway belonging to the Paleo-Tethys Ocean existed between North and South China during the Paleozoic, connecting the two major oceans (Fig. 1a). Geological processes within the tectonic realm of this seaway involved subduction, arc formation, back-arc extension, and the final continental collision that welded North and South China and formed the composite Paleozoic–Mesozoic Central China Orogenic belt (Liu et al., 2011; Wu and Zheng, 2013; Zhang et al., 2004; Yin and Nie, 1993). This orogenic belt is further divided into different sections and each of them exhibits different evolutionary histories (Qinling–Tongbai–Hong'an–Dabie–Sulu; Fig. 2) (Liu et al., 2011; Wu and Zheng, 2013; Zhang et al., 2004). The western section (Qinling–Tongbai–Hong'an) of the orogen shows significant Paleozoic arc–continental collisions and the final continental collisions caused mainly amphibolite facies metamorphism in the southern Qinling section during the Triassic (Fig. S1A) (Dong et al., 2011; Wu, 2009; Zhou et al., 2011, 2015). Alternatively, the eastern section (Dabie-Sulu) exhibits more obvious features

of continental collision between the two major continental blocks, whose ultrahigh pressure eclogites give mainly Triassic metamorphic ages and indicate Triassic continental collisional events (Fig. S1A) (Okay et al., 1989; Wang et al., 1989, 1992; Xu et al., 1992; Ye et al., 2000). Previous studies generally seem to show that the final collision of North and South China, which completely disconnected the northern seaway, occurred during the Triassic (An et al., 2018; Dong et al., 2016; Meng and Lin, 2021; Meng and Zhang, 1999; Wu and Zheng, 2013). If so, this age would apparently follow the time of the end-Permian extinction. However, the restriction of circulation of oceanic water masses does not wait until the final continental collision, and will already initiate with initial collision and the onset of crustal thickening. Besides, geochronological results from high-grade rocks tend to post-date the onset of orogenic belts, because most metamorphic zircon grains form during post-peak retrograde metamorphic stages (Roberts and Finger, 1997; Zhao et al., 2015a). On the other hand, paleontological studies found similar Late Paleozoic and Mesozoic floras and faunas in both North and South China (Metcalfe, 1998, 2006; Şengör and Atayman, 2009), requiring land bridges between them and implying an early amalgamation of these continental blocks. Similar results are also indicated by paleomagnetic data (Fig. 1b) (Huang et al., 2018). Based on these considerations, it is suggested that the age of the onset of the continental collision between North and South China needs to be critically reevaluated.

Samples of this study were collected from the Beihuaiyang zone in the northernmost paft of the Dabie orogenic belt (Fig. 2 and Fig. S1B), and the Qushan Island located on the continental shelf region of the northeast Cathaysia, South China (Fig. 2). The metamorphic rocks of the Beihuaiyang zone did not undergo deep subduction, and compared with the deeply subducted eclogite facies rocks which were then exhumed to the surface, metamorphism of these metamorphic rocks is more likely to represent the earlier phases of the continental collisional events and give more precise constraints on the initial docking of the two continental blocks. The Foziling Group and the Luzhenguan Complex are the two major constituent lithological units of the Beihuaiyang zone, with both units having close affinity with the Yangtze block of South China (Chen et al., 2003; Wu et al., 2007; Zheng et al., 2005). The metamorphism they record are the direct result of the convergence between these two continental blocks. Two garnet mica schist samples (FT4-1 and -2) from the Foziling Group, one garnet-bearing granitic gneiss sample (19HS03), and one fine-grained biotite gneiss sample (FT2, Fig. S1B) from the Luzhenguan Complex were dated. Sampling locations, detailed descriptions of these samples, and analytical results are included in the Supplementary material 1. Representative photomicrographs and dating results are presented in Figure 3. The mineral assemblage of Grt + Bt + Ms + Pl + Chl + Ep + Qtz in the garnet mica schist samples suggests greenschist to amphibolite facies metamorphism (Fig. 3).

The high-grade metamorphic rocks of the Qushan Island in South China include garnet amphibolites, garnet biotite gneiss, garnet sillimanite gneiss, and marble, all of which exhibit obvious features of anatexis and strong deformation. We identified a high-pressure granulite facies mineral assemblage of garnet + kyanite + sillimanite + K-feldspar + plagioclase + quartz from the garnet biotite gneiss occurring on Qushan Island (Fig. 4a), indicating high-grade metamorphism similar to that of the northern Wuyi terrane during the Permo–Triassic orogeny. One garnet sillimanite biotite gneiss sample (14CS01) and one leucogranitic vein sample (14CS02) were collected from this region. Detailed descriptions of the collected Qushan Island samples and other related rocks of the region are presented in the Supplementary material 2.

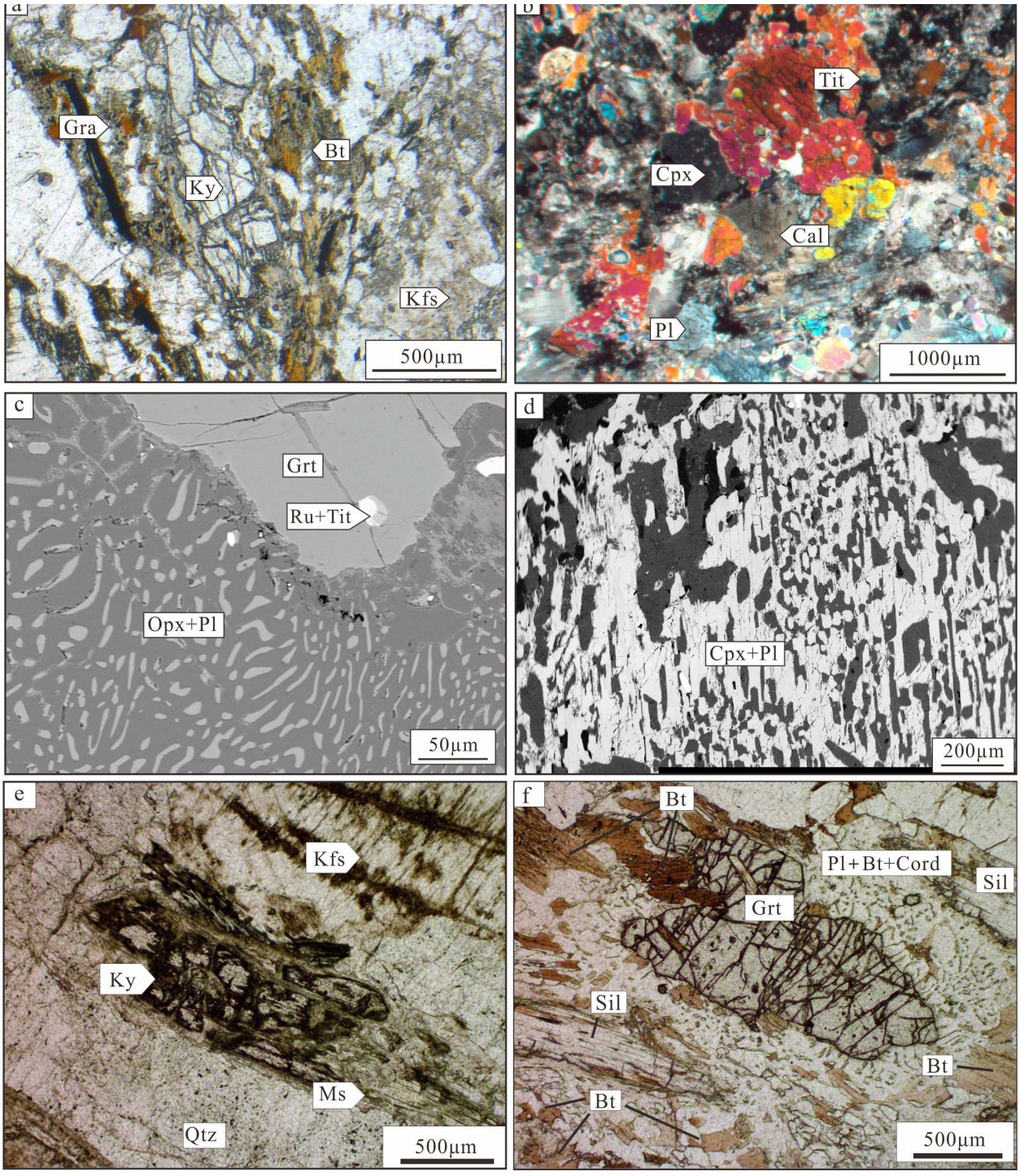

271

272 **Fig. 4.** Representative photomicrographs of high-grade metamorphic rocks from the Wuyi
273 terrane and Qushan Island of the South China intracontinental orogenic belt. (a) Pelitic high
274 pressure granulite sample collected from the Qushan Island of northern Wuyi. (b)
275 Metamorphosed calc-silicate sample collected from the Qushan Island. (c-d) Mafic granulite and
276 retrograded eclogite samples from the Wuyi terrane, showing symplectitic reactions textures
277 formed during decompressional retrograde metamorphic stages: Opx + Pl replacing garnet (c)
278 and Cpx + Pl replacing Omph (d) (modified from Zhao et al. (2017). (e-f) Pelitic granulite

samples from the Wuyi terrane (modified from Zhao et al. (2018). Mineral abbreviations: Opx – orthopyroxene, Ru – rutile, Tit – titanite, Cpx – clinopyroxene, Sil – sillimanite, Ky – kyanite, Cord – cordierite, Gra – graphite, Cal - calcite. Others are as in Fig. 3.

3 Analytical methods

The collected samples were crushed and separated by standard density and magnetic techniques. Rutile, titanite, and zircon were handpicked under a microscope. Rutile samples with rutile standards DXK (1782.6 ± 2.8 Ma, Li et al., 2013a) and JDX (518 ± 4 Ma, Li et al., 2013a), titanite samples with standards YQ82 (1837.6 ± 1.0 Ma; Huyskens et al., 2016) and Ontario (1053.5 ± 3.1 Ma; Spencer et al., 2013) were put together in epoxy mount, respectively. The mounts were polished to expose the mid-sections of crystals. Zircon samples were mounted in the epoxy with zircon standard of Plešovice (337.1 ± 0.4 Ma, Sláma et al., 2008) and Qinghu (159.5 ± 0.2 Ma, Li et al., 2013b). In order to keep the thin overgrowth zircon rim, we did not polish those zircon crystals but cleaned them carefully. Single-minerals U–Pb age analysis were carried out using Secondary Ion Mass Spectrometry (CAMECA IMS 1280HR) at Institute of Geology and Geophysics, Chinese Academy of Sciences.

Rutile SIMS U–Pb dating: The O_2^- was selected to be the primary beam, which was accelerated at a potential of –13 kV. The intensity of primary beam was about 10–15 nA. The size elliptical analytical spot was 20 × 30 μm. Positive secondary ions were extracted with a +10 kV potential. One electron multiplier was used to count secondary ions in peak-jumping mode. The time of pre-sputtering was set as 120 s to remove the coated gold layer. The time duration for each spot analysis is about 15 min. The detailed analytical procedures can be found in Li et al. (2011). Rutile standard DXK was used to calibrate the instrument fractionation between U and Pb, and standard JDX was used as an unknown sample to assess the quality of calibration. Data without common lead correction was plot on Tera-Wasserburg concordia diagrams to obtain the lower intercepted age with the concordia curve. The age of single point was after ^{207}Pb correction of common lead.

Titanite SIMS U–Pb dating: The primary beam of O_2^- was accelerated at a potential of –13 kV. The intensity of the primary beam was 10–17 nA. The analytical beam was 20 × 30 μm in size. It took 120 s for pre-sputtered and 17 min for each spot analysis. The secondary ions were counted by an electron multiplier in peak-jumping mode (Li et al., 2011). The counts of $^{56}Fe^{16}O^+$ were used to calibrate the matrix effect of titanite SIMS U–Pb dating. The calibration formula is $(^{206}Pb^+/^{238}U^+)_{calibrated} = (^{206}Pb^+/^{238}U^+)_{measured} /(^{56}Fe^{16}O^+/PB)^{-0.11}$, in which the PB is the intensity of primary beam. The instrument fractionation between U and Pb for titanite sample is calibrated using titanite standard YQ82, and the quality of calibration is reference to the calibration age results of titanite standard Ontario.

Unpolished zircon SIMS U–Pb dating: The elliptical analytical spot was 10 × 15 μm in size. Since the analyzed zircon grains were not polished, the time of pre-sputtered was increased to 180 s to remove the contamination of common lead. The total time duration of single point analysis is ~15 min. Zircon standard Plešovice was used for U/Pb instrument fractionation calibration, and zircon standard Qinghu was used as an unknown sample to monitor the quality of data. The common Pb calibration was performed using the value of ^{204}Pb. The detailed description of SIMS zircon U–Pb dating method is described in Li et al. (2009).

Uncertainties of all isotopic ratios are reported at 1σ level, and the age are quoted with 95% confidence intervals.

SHRIMP zircon U-Pb age dating: SHRIMP zircon U-Pb age dating were carried out at Beijing SHRIMP Center, Chinese Academy of Geological Sciences, using the SHRIMP II instrument. The focused O2- beam is ~4nA and the standard to unknown ratio is 1:4. Five scans wree used for each analysis. The analytical protocol and procedues have been detailed described by Williams (1998). Commen Pb corrections were based on the measured 204Pb. Uncertainties for individual analyses are quoted a 1σ.

Trace elements of rutile and titanite: Analyses of mineral trance elements were performed using Agilent 7500a Inductively Coupled Plasma Mass Spectrometer coupled with 193 nm ArF-excimer laser-ablation system at Institute of Geology and Geophysics, Chinese Academy of Sciences. The analytical laser beam size was 32 μm. The detailed analytical conditions could be referenced to Wu et al. (2018). NIST SRM 610 was used to calibrate the measured data, and USGS BCR-2G was as the data calibration quality monitoring sample. The internal standard elements for trace element content correction are Ti for rutile and Si for titanite.

4 Results

4.1 Analytical results of the northern Dabie samples

Detailed analytical results of the sample from the Beihuaiyang zone of the northern Dabie orogeny are presented in Supplementary materal 1 and Fig. 3. The rutile grains in the two garnet-mica schist samples range from 50 to 150 μm in length. The high Nb and low Cr contents, together with low Cr/Nb ratios (0.03–0.36) (Fig. S2 and Table S1) show that these rutile grains grew during metamorphism in the metapelite rocks (Meinhold, 2010). The Zr contents of rutile in FT4-1 and FT4-2 are 87–116 ppm (mean = 104 ppm) and 102–126 ppm (mean = 112 ppm), respectively, corresponding to metamorphic temperatures of 530–551 °C and 542–557 °C (Hayden et al., 2008, Table S1). The yielded rutile U–Pb ages for FT4-1 is 268 ± 6 Ma (MSWD = 1.6) and for FT-2 is 264 ± 6 Ma (MSWD = 0.94) (Figs. 3d and 3e, Table S2).

Most titanite grains in granitic gneiss sample 19HS03 are homogeneous as shown in BSE images (Fig. S3), with Al_2O_3 = 6.48–8.04 wt.%, Fe_2O_3 = 0.99–1.50 wt.%, Al/Fe = 7.0–12.2, Zr = 14–24 ppm. The Zr-in-titanite temperatures are estimated to be 611–635 °C (Table S3), but maybe overestimated because of the absence of rutile and ilmenite in rock (Hayden et al., 2007). The U–Pb age of homogeneous titanite is 266 ± 3 Ma (MSWD = 1.5; Fig. 3f, Table S4), with U contents of 2–36 ppm, and Th/U ratios of 0.01–0.07. A few titanite grains display complex zoning, but show no systematic compositional variations (Figs. S3 and S4). The Al_2O_3 and Fe_2O_3 contents for these grains are 4.96–7.88 wt.% and 0.95–2.10 wt.%, respectively, with Al/Fe = 4.1–12.9. The Zr contents in titanite cores are 26–43 ppm, and the calculated Zr-in-titanite temperatures are 638–659 °C. Both types of titanite grains have high Al/Fe ratios (Fig. S4, Table S3), which indicate that they were formed during metamorphism (Aleinikoff et al., 2002). The U–Pb age of titanite core is 376 ± 8 Ma (MSWD = 1.9; Fig. 3f, Table S4), with U = 2–36 ppm and Th/U = 0.01–0.07.

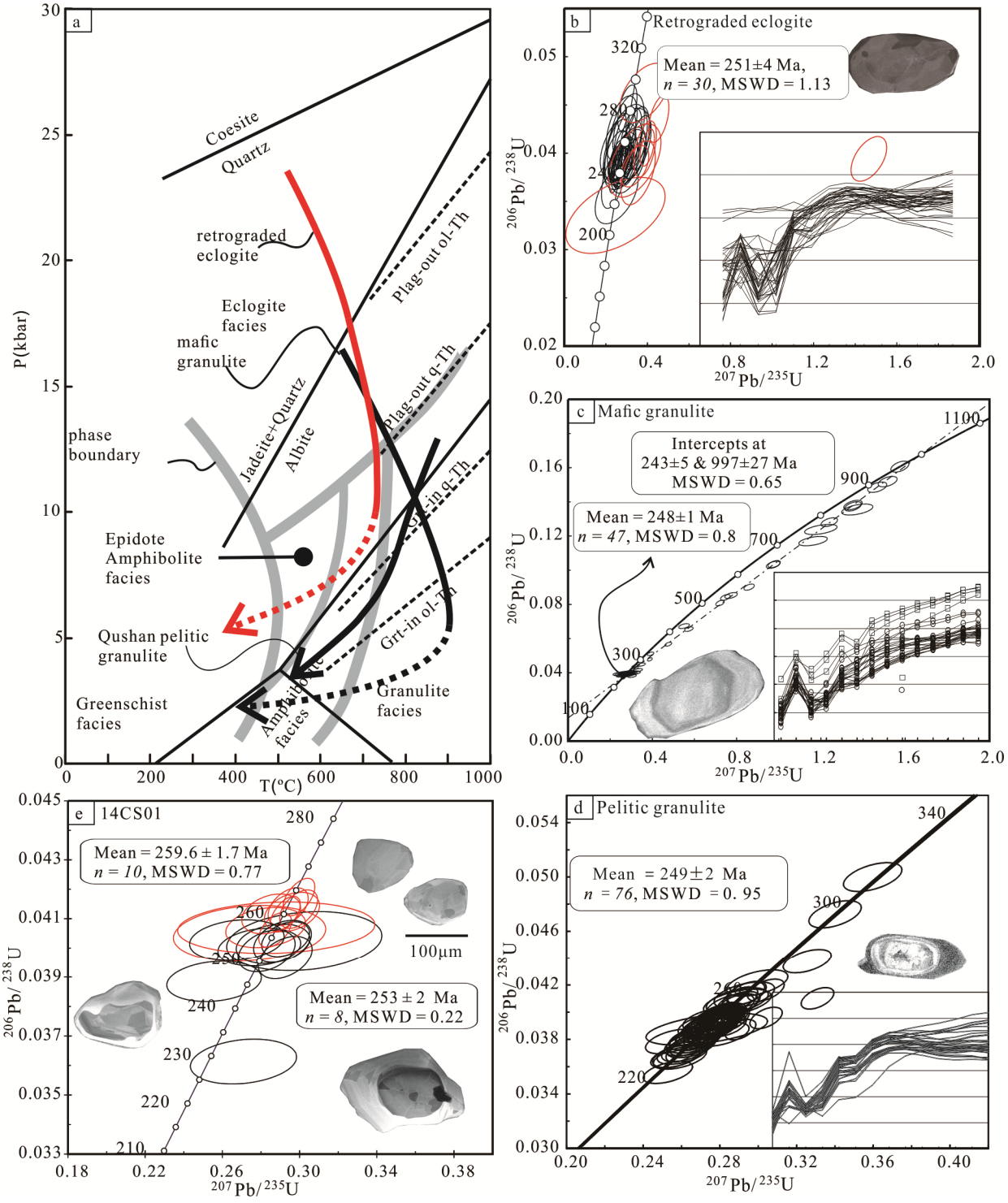

Fig. 5. (a) Metamorphic P-T paths of Permo-Triassic metamorphic rocks in northern Wuyi terrane and Qushan Island. *P–T* paths of mafic granulite and retrograded eclogite are from Zhao et al. (2017) and that of the Qushan Island is from Cao et al. (2022). Zircon U-Pb age dating results of the high-grade rocks from northern Wuyi (b-d) and Qushan Island (e). Zircon age dating results of retrograded eclogite and mafic granulite (b-c) are from Zhao et al. (2017) and those of the politic granulite (d) is from Zhao et al. (2018).

The metamorphic overgrowth rims of zircon grains are mostly too thin for traditional analysis (Fig. 3g, S5). In this study, we directly analyzed the zircon surface without polishing them to measure the U and Pb isotopes. The unpolished zircon grains in two of the paragneiss samples (FT2 and FT4-1) are analyzed. After excluding data with high common Pb and large error of isotopic ratios, there are 54 and 45 reliable age results for samples FT2 and FT4-1, respectively (Table S5). Four unpolished zircon grains in FT2 show Th/U < 0.1, and yielded apparent $^{206}Pb/^{238}U$ ages of 266 ± 6, 274 ± 22, 279 ± 6, and 255 ± 12 Ma (1σ), with U contents of 623, 959, 425, and 1162 ppm, respectively. The weighted mean average age is 270 ± 8 Ma (MSWD = 1.4; Fig. S6A). Three unpolished zircon grains in FT4-1 yielded young apparent $^{206}Pb/^{238}U$ ages of 259 ± 6, 266 ± 5, and 268 ± 7 Ma (1σ), with U contents of 1759, 2252, and 333 ppm, respectively. The weighted mean average age is 264 ± 7 Ma (MSWD = 0.6; Fig. S6B). All the 7 young age results in the two sample gave a weighted mean average age of 267 ± 5 Ma (MSWD = 1.2; Fig. 3g).

4.2 Analytical results of the South China samples

Analytical results (SHRIMP zircon U-Pb) of the South China samples, including the garnet sillimanite biotite (14CS01) and the leucogranitic vein (14CS02), are included in Supplementary materal 2. These zircon grains exhibit typical metamorphic features, like sector zoning or without any zoning (Figs. S2.4A and B). Some of the zircon grains show core-rim structures, with both of them exhibiting typical metamorphic features (Fig. 5a). Analyzed results of these two samples are similar. Apparent ages of zircon cores from both samples are older than those of zircon rims. Apparent $^{206}Pb/^{238}U$ ages of the 20 analyzed spots from sample 14CS02 are 246 – 262 Ma while these of sample 14CS01 are mostly 246 – 264 Ma. Age results of both samples show two clusters, one at ~260 Ma and the other at ~252 Ma, with the former from zircon cores and the latter from other zircon domains (Figs. S2.4A and B). An older age of ~260 Ma and a younger age of ~253 Ma are yielded from the garnet sillimanite biotite sample, which were interpreted to represent the time of two episodes of metamorphism (Fig. 5a).

5 Discussion

5.1 Permo-Triassic metamorphism related with crustal thickening event along the East Asian continent

Bordered to the southeast by the Sulu orogenic belt, the Jiaobei Terrane is part of the North China craton with early Precambrian crystalline basement components (Fig. 2) (Jahn et al., 2008; Liu, P. et al., 2012; Wu, M. et al., 2014; Liu F.L., et al., 2014). These components record Archean and Paleoproterozoic high-grade metamorphism during the amalgamation and cratonization of North China (Liu, P. et al., 2012; Wu, M. et al., 2014; Liu F.L., et al., 2014). The meta-sedimentary rocks of the Jingshan and Fenzishan groups occur in the southern part of the Jiaobei Terrane, in direct contact with the Sulu ultrahigh pressure orogenic belt. Part of the Jingshan and Fenzishan Group rocks were subjected to the Permo–Triassic orogenic event due to the continental collision of the North and South China (Liu et al., 2018; Cao et al., 2016). As described by Liu et al. (2018), the quartz schist and muscovite schist samples of the Jingshan Group both show Paleoproterozoic metamorphism, at 1905 Ma and 1862 Ma, respectively (Fig. 6). Besides, the muscovite grains from these samples gave Late Permian $^{40}Ar/^{39}Ar$ plateau ages of 252.1 – 251.1 Ma (Fig. 6). These Late Permian metamorphic ages represent the time of crustal

409 thickening in the southern North China Craton, due to the interactions between the North and
410 South China in Late Permian.

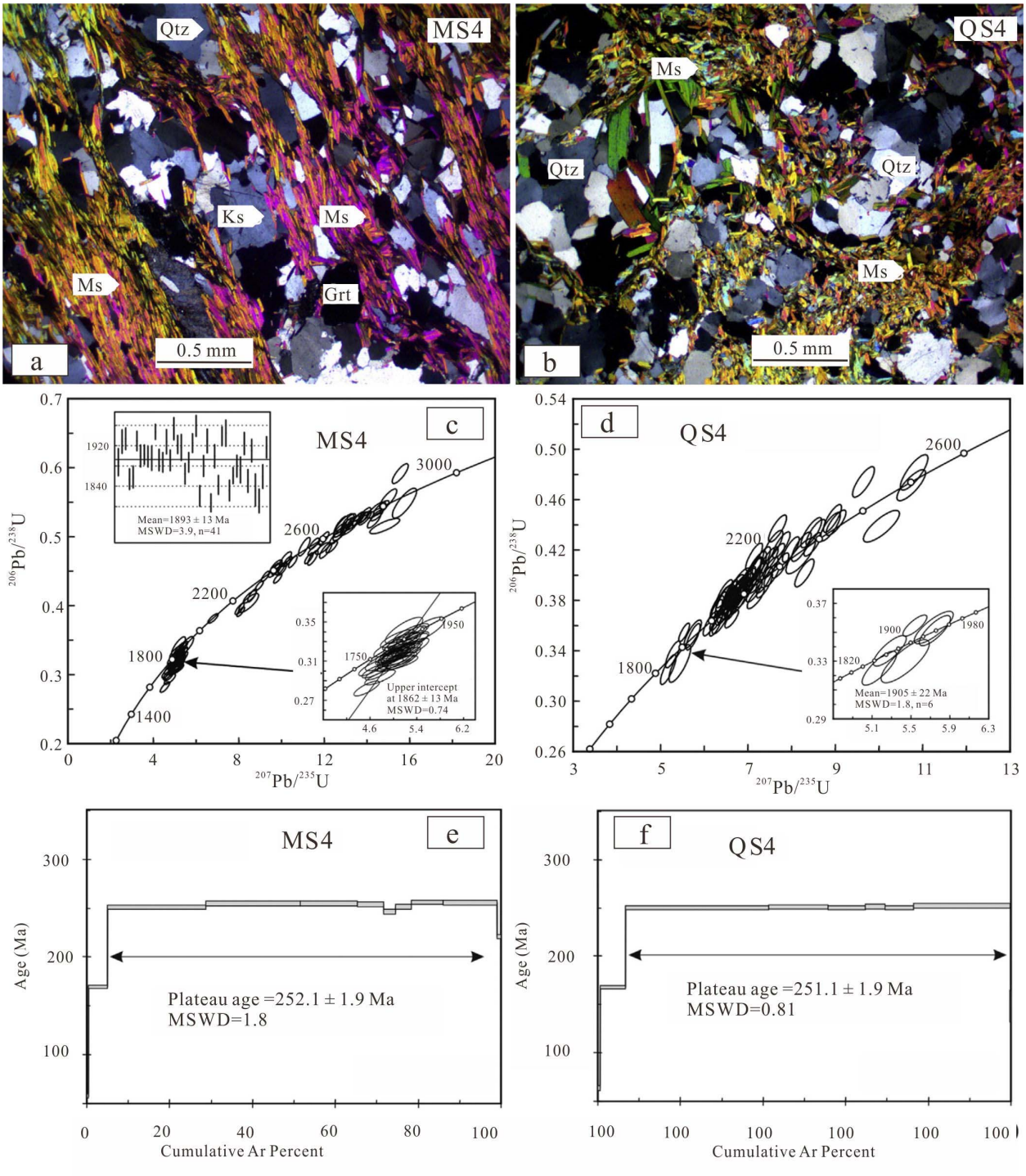

411

412 **Fig. 6.** Representative photomicrographs and dating results of the samples from the Jingshan
413 Group of the Jiaobei Terrane in the southeastern North China craton. The muscovite schist

(MS4) and quart schist (QS3) samples record both Paleoproterozoic and Late Permian metamorphism. These images are from Liu et al., 2018.

The South China Permo–Triassic intracontinental orogeny affected most areas of the Cathaysia block, as indicated by pervasive deformation and magmatism (Huang, 1960; Li et al., 2006, 2017a, 2017b; Li and Li, 2007; Lin et al., 2018; Wang et al., 2013b; Xiao and He, 2005; Zhang et al., 2017). These geological records led Hsü et al. (1988) to propose that continental collisional events occurred within South China, which received extensive criticism (Chen et al., 1991; Gupta et al., 1989; Rowley et al., 1989). Currently, the widespread Permo-Triassic deformation and magmatism in the Cathaysia block are generally believed to have occurred in an intracontinental environment that resulted from far-field stress derived from the Central China Orogenic belt and/or the continental collision between South China and Indochina (Li et al., 2016; Song et al., 2015; Wang et al., 2012, 2013b, 2021; Zhang et al., 2013a), and/or the subduction of the Paleo-Pacific plate (Chu et al., 2012; Li et al., 2012a, 2012b; Li and Li, 2007; Mao et al., 2013). One particular aspect of the Permo–Triassic orogeny in South China that has been overlooked by many previous studies is the significant crustal thickening in the Wuyi segment of the northeast regions of the Cathaysia block. This segment of the intracontinental orogen is parallel with the Sulu orogenic belt (Fig. 2) and the far-field stress derived from the latter has been suggested to be a major driver of its formation (Zhao et al., 2022). Despite the strong deformation, Permo–Triassic high-grade metamorphism involving middle- to lower-crust has been rarely reported from the Cathaysia block, with most deformation involving only upper-crustal level components, as indicated by thrusting and brittle deformation (Wang et al., 2012; Zhang et al., 2013a). The identification of Permo–Triassic retrograded eclogites and high-pressure granulites from the northeastern Cathaysia block imply that this Permo–Triassic orogeny is strong enough to have also affected lower crustal components (Xia et al., 2021; Zhao et al., 2017, 2018). Both these mafic rocks and the metasedimentary rocks preserve high-pressure granulite facies mineral assemblages of garnet + clinopyroxene + orthopyroxene + plagioclase + quartz, and garnet + kyanite + sillimanite + biotite + K-feldspar + plagioclase + quartz, respectively (Fig. 4). Decompressional reaction textures around garnet grains in the mafic and pelitic granulites (Fig. 4; the intergrowths of fine-grained clinopyroxene + plagioclase, and orthopyroxene + plagioclase in mafic granulites and intergrowth of plagioclase + cordierite + biotite in pelitic granulites) indicate significant uplift during later retrograde metamorphic stages. Eclogite facies metamorphic conditions and clockwise *P–T* paths were extracted from these rocks, with metamorphic peak pressures of ~23–24 Kbar (Fig. 5e) (Zhao et al., 2017). Zircon U-Pb dating of these high-grade rocks indicates Triassic metamorphic ages of 251–248 Ma (Figs. 5b, c and d, Zhao et al., 2017).

The South China Permo–Triassic high-grade metamorphism is not just confined to the northern Wuyi terrane (Fig. 2, Zhao et al., 2022), but also occur in the Yunkai terrane situated in the southwest Cathaysia block, with Triassic metamorphic ages varying between 251 Ma and 230 Ma (Fig. 2) (Zhao et al., 2015b). The Permo–Triassic high-grade metamorphic rocks identified from the Qushan Island represent the northeast extension of the Permo-Triassic orogenic event in northeast South China (Fig. 2). SIMS zircon U-Pb age dating results of the high-grade metamorphic rocks of the Qushan Island show Permian metamorphic ages of ca. 260 Ma (Fig. 5a), consistent with previously published data (Cao et al., 2022; Jiang et al., 2016). Thus, Permo–Triassic metamorphism of eastmost Cathaysia occurred earlier than the formation of the high-grade rocks in the inland regions mentioned above and firmly indicates a Permian

459 onset of the South China Permo–Triassic intracontinental orogeny. For the metamorphic rocks of
460 the Beihuaiyang zone in northern Dabie orogenic belt, SIMS rutile U-Pb dating of the two garnet
461 mica schist samples give consistent Permian metamorphic ages of ca. 265 Ma (Figs. 3d and e).
462 SIMS titanite U-Pb dating of the garnet-bearing granitic gneiss sample gives a Permian
463 metamorphic age of 266 Ma (Fig. 3f). SIMS zircon U-Pb dating on the unpolished thin (~2μm)
464 metamorphic zircon rims of the garnet mica schist and the fine-grained biotite gneiss samples
465 shows uniform Permian metamorphic ages of ca. 267 Ma (Fig. 3g). Considering that such low-
466 grade metamorphism is the result of crustal thickening due to continental collision, these
467 metamorphic ages thus appear to indicate a Middle Permian initiation of the Dabie–Sulu
468 orogenic belt, or even earlier. To sum up, Permian metamorphic ages, which are all closely
469 related with crustal thickening because of the continental collision between the South and North
470 China, have been identified from the southern North China, the northern Dabie orogen and the
471 South China. These Permian metamorphic ages collectively indicate Permian crustal thickening
472 events along East Asian continent.

473 **5.2 Permian initiation of the continental collision and restrictions on oceanic circulations**

474 There is currently a paradox between the paleogeographic reconstructions of South China and
475 neighboring continents as based on evidence from paleontological and geological studies.
476 Paleontological affinities argue that North and South China amalgamated before the Permian
477 mass extinction, depicting a united landmass for the "Cathaysian" biota as well as isolating the
478 Paleo-Tethys from the Panthalassa Ocean with this united land bridge (Algeo et al., 2010; Algeo
479 and Twitchett, 2010; Metcalfe, 1998, 2006; Şengör and Atayman, 2009). On the other hand,
480 previous studies of regional tectonics suggest that the final amalgamation occurred during the
481 Triassic, postdating the end-Permian extinction (An et al., 2018; Dong et al., 2016; Meng and
482 Lin, 2021; Meng and Zhang, 1999; Wu and Zheng, 2013).

483 The continental collision between North and South China is the most significant tectonic event
484 that occurred in East Asia during the Paleozoic–Mesozoic (Yin and Nie, 1993; Liu et al., 2011;
485 Wu and Zheng, 2013; Zhang et al., 1996, 2004; Meng and Zhang, 1999). This event not only
486 resulted in the ultrahigh pressure metamorphism in the Central China Orogenic belt, but also
487 caused crustal thickening events in both North and South China, like the Permo–Triassic
488 intracontinental orogeny in South China (Zhao et al., 2022). Crustal thickening of the southern
489 North China is implied by the Late Permian metamorphic overprinting shown by the early
490 Precambrian basement components of the Jiaobei Terrane, and the initiation of crustal thickening
491 should predate their Late Permian Ar-Ar age of ca. 252 Ma (Fig. 6, Liu et al., 2018). The
492 Beihuaiyang zone in northern Dabie orogen was not subjected to deep subduction and the
493 geochronological dating of samples from the Beihuaiyang zone gives coherent metamorphic ages
494 of ca. 267 Ma (Fig. 3). The metamorphism recorded by these lithological units indicates that they
495 were transported to mid-crustal level during continental collision. Their metamorphic ages
496 indicate crustal thickening during the Permian, prior to crustal thickening in southeastern North
497 China.

498 Permo–Triassic high-grade metamorphism within the Wuyi segment of the South China
499 intracontinental orogen substantiates the Permian continental collision between North and South
500 China from another perspective. The northeast–southwest striking Wuyi segment of the
501 intracontinental orogenic belt is sandwiched by the Dabie–Sulu orogenic belt to the north (and

northwest) and by the the Paleo-Pacific subduction zone to the southeast (Fig. 2). Both these plate-boundary interactions contributed to the formation of this intracontinental orogeny, but the Dabie–Sulu orogenic belt was the major driver (Zhao et al., 2022; Chu et al., 2012; Li et al., 2012a, 2012b; Li and Li, 2007; Mao et al., 2013). The high-grade metamorphism on Qushan Island of the northern Wuyi orogenic belt at ca. 260 Ma apparently predates the Triassic UHP eclogite facies metamorphism along the Dabie–Sulu orogenic belt, but postdates the Permian metamorphism of northern Dabie orogenic belt as shown by the metamorphic rocks within the Beihuaiyang zone. From northeast to southwest, high-grade metamorphism of the Wuyi intracontinental orogen shows a younging trend (Fig. 2). Such a younging trend suggests that the onset of the intracontinental orogeny started from the northeast of South China and propagated to the southwest. This inferred geometry of the intracontinental orogenic belt is consistent with the generally accepted model of the Central China Orogenic belt, where the amalgamation of North and South China initiated in the east and gradually propagated to the west (Fig. 1b) (Gilder et al., 1999; Huang et al., 2018; Oh, 2015; Yin and Nie, 1993).

Based on our synthesis and new data, we propose a new tectonic model for the amalgamation of North and South China during the Permo–Triassic (Fig. 7). The prior South China Paleozoic Orogeny (ca. 460–410 Ma) stabilized most of South China after the Neoproterozoic Nanhua rift (Li et al., 2017a; Wang et al., 2013b), which left behind a lithospheric weak zone (Fig. 7b) (Zhao et al., 2022). Initial continental collision between North and South China occurred along the Dabie–Sulu orogenic belt (eastern segment of the Central China Orogenic belt), resulting in the crustal thickening in the Beihuaiyang zone and also in southeastern North China (the low-grade metamorphism of Beihuaiyang zone at ca. 267 Ma; Fig. 7c). Far-field stress derived from the Dabie–Sulu orogenic belt in the north, as well as the convergence of the paleo-Pacific plate in the southeast facilitated the formation of the Wuyi intracontinental orogenic belt along the pre-existing lithospheric weak zone (Fig. 7d) (Li et al., 2006; Zhao et al., 2022). Metamorphic ages of the high-grade rocks in different regions of this orogenic belt show that the onset of this orogeny started in the northeast and then propagated westward (Huang et al., 2018; Yin and Nie, 1993). Continued continental collision between North and South China along the Dabie–Sulu orogenic belt caused significant tectonic stress, which not only resulted in the deep subduction of the Yangtze continental crust underneath the southern margin of North China, but also stabilized the lithospheric weak zone within South China, forming the Permo–Triassic intracontinental orogenic belt (Fig. 7). Significant crustal thickening occurred in the Wuyi terrane of Cathaysia, parallel with the Sulu orogenic belt (Fig. 2).

The Permo–Triassic orogenic belts in southeastern North China, within South China, and along the Dabie-Sulu orogen thus effectively isolated the Paleo-Tethys Ocean from the Panthalassa Ocean along the whole eastern front of Eurasia. Ocean circulation became severely restricted between these once contiguous oceans (Fig. 7a). Based on this refined timing of orogenic events, restricted ocean circulation between the Paleo-Tethys Ocean and the Panthalassa therefore occurred in Permian time and thus likely played a preconditioning role for the severity of the Permian mass extinction in the critical region. This restriction might also suggest a role for the Panthalassa Ocean in providing refugia for Triassic survivors and biospheric recovery. This new tectonic model of the Paleo-Tethys realm and its role in leadup to the end-Permian extinction in the region is in good accordance with the distinct features of the two Permian oceans as well as their paleontological records. From a continental perspective, the collision of North and South China also represents the final uniting of major continental blocks during the time of

supercontinent Pangea and the formation of the subduction girdle around the supercontinent (Fig. 7a) (Li et al., 2019). With a deathly combination of both restricted global ocean circulation and a huge amount of volcanic emissions from the ring of fire (subduction girdle), the occurrence of a global biospheric crisis at this time is perhaps not surprising.

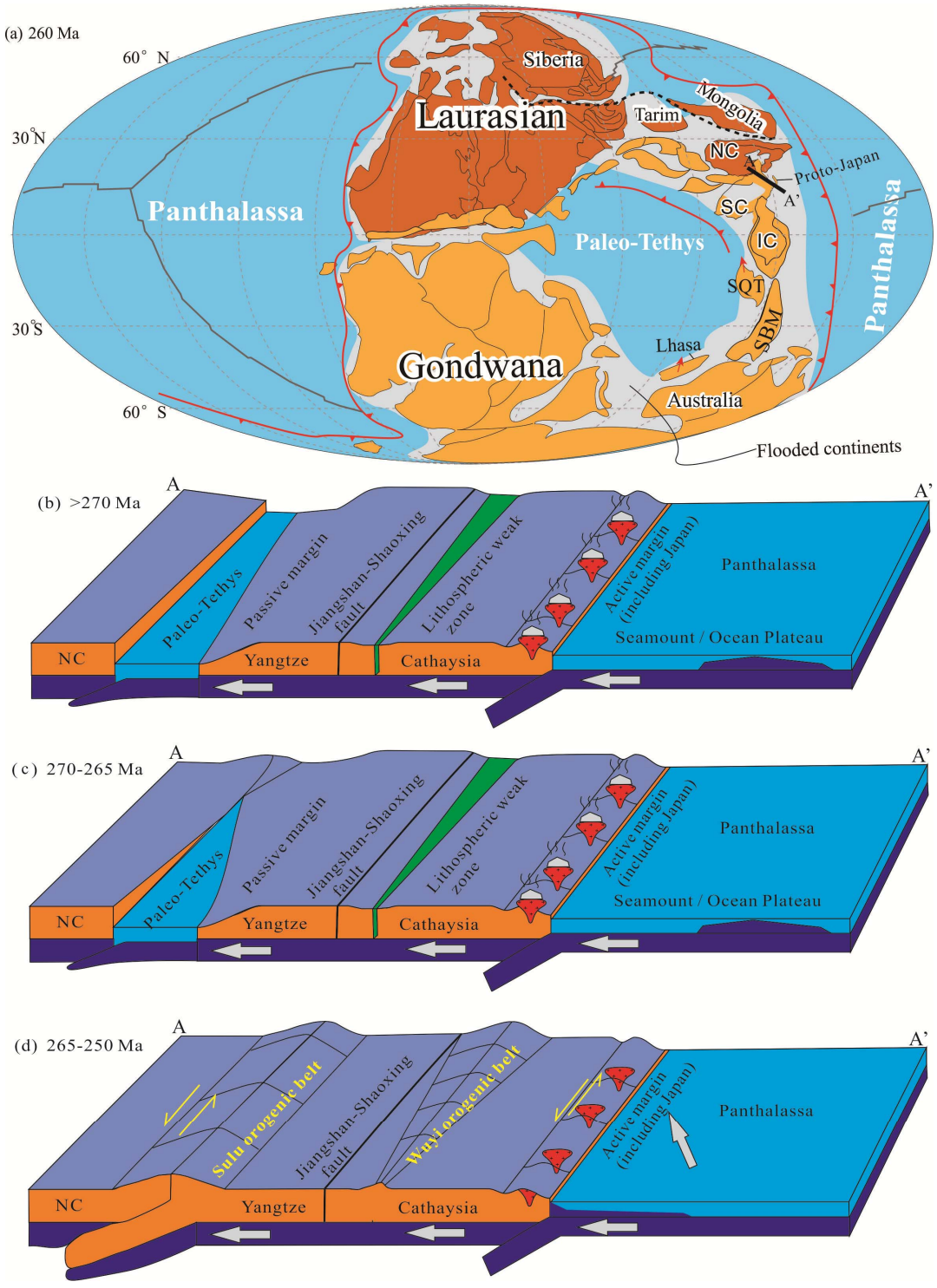

551

552 **Fig. 7.** (a) Late Permian reconstruction of Laurasia. Note the proximity of North and South
553 China shown here, unlike in the reconstruction of Figure 1a, is advocated in this study to have
554 been already established by ca. 260 Ma, i.e., in the leadup to the Permian mass extinction.
555 Modified after Wu et al. (2020). (b-d) Tectonic model showing the amalgamation of the North
556 and South China blocks, and the formation of the South China Permo-Triassic intracontinental
557 orogen in the Wuyi terrane. NCC – North China craton.

558 ## 6 Conclusions

559 Permo–Triassic metamorphism due to crustal thickening in southeastern North China, the
560 intracontinental orogeny of South China, and low-grade metamorphism in the northern Dabie
561 orogenic belt were all results of the amalgamation of North and South China in East Asia.
562 Therefore, while the timing of the low-grade metamorphism in the northern Dabie orogenic belt
563 provides direct evidence for the amalgamation process, the initiation of the intracontinental
564 orogeny in South China and crustal thickening in southeastern North China can independently
565 substantiate the initial timing of Permian amalgamation from other perspectives. Metamorphic
566 ages of lithologies from these different localities provide coherent clues for Middle Permian
567 continental collision (ca. 270 Ma), rather than during Triassic as previously suggested based on
568 exhumed ultrahigh pressure eclogite facies rocks. Thus, continental collisions and the formation
569 of orogenic belts in East Asia isolated the Paleo-Tethys Ocean from the Panthalassa Ocean
570 before the end-Permian mass extinction. After this isolation, the poorly mixed Paleo-Tethys
571 Ocean gradually became a dead sea, thereby preconditioning and facilitating the end-Permian
572 biospheric crisis in the region.

573 ## Acknowledgments

574 The authors declare no conflicts of interest.
575 The manuscript benefitted from discussions with Profs. Xianhua Li. Xiaoxiao Ling, Guoqiang
576 Tiang, and Yu Liu helped with analysis. This work was funded by the National Natural Science
577 Foundation of China (grant nos. 41872197 and 41890834).

578

579 ## References

580 Aleinikoff, J. N., Wintsch, R. P., Fanning, C. M. & Dorais, M. J. 2002. U-Pb geochronology of zircon and
581 polygenetic titanite from the Glastonbury Complex, Connecticut, USA: an integrated SEM, EMPA, TIMS, and
582 SHRIMP study. *Chemical Geology* **188**, 125-147.
583 Algeo, T., Shen, Y., Zhang, T., Lyons, T., Bates, S., Rowe, H. & Nguyen, T. K. T. 2008. Association of34S-depleted
584 pyrite layers with negative carbonateδ13C excursions at the Permian-Triassic boundary: Evidence for upwelling
585 of sulfidic deep-ocean water masses. *Geochemistry, Geophysics, Geosystems* **9**, doi:10.1029/2007GC001823.
586 Algeo, T. J., Hinnov, L., Moser, J., Maynard, J. B., Elswick, E., Kuwahara, K. & Sano, H. 2010. Changes in
587 productivity and redox conditions in the Panthalassic Ocean during the latest Permian. *Geology* **38**, 187-190.
588 Algeo, T. J., Kuwahara, K., Sano, H., Bates, S., Lyons, T., Elswick, E., Hinnov, L., Ellwood, B., Moser, J. &
589 Maynard, J. B. 2011. Spatial variation in sediment fluxes, redox conditions, and productivity in the Permian–
590 Triassic Panthalassic Ocean. *Palaeogeography, Palaeoclimatology, Palaeoecology* **308**, 65-83.
591 Algeo, T. J. & Twitchett, R. J. 2010. Anomalous Early Triassic sediment fluxes due to elevated weathering rates and

592 their biological consequences. *Geology* **38**, 1023-1026.
593 An, S.-C., Li, S.-G. & Liu, Z. 2018. Modification of the Sm-Nd isotopic system in garnet induced by retrogressive
594 fluids. *Journal of Metamorphic Geology*, DOI: 10.1111/jmg.12426.
595 Burgess, S. D. & Bowring, S. A. 2015. High-precision geochronology confirms voluminous magmatism before,
596 during, and after Earth's most severe extinction. *Science Advances* **1**, e1500470.
597 Cao, C., Love, G. D., Hays, L. E., Wang, W., Shen, S. & Summons, R. E. 2009. Biogeochemical evidence for
598 euxinic oceans and ecological disturbance presaging the end-Permian mass extinction event. *Earth and Planetary*
599 *Science Letters* **281**, 188-201.
600 Cao, C. & Zheng, Q. 2009. Geological event sequences of the Permian-Triassic transition recorded in the
601 microfacies in Meishan section. *Science in China Series D: Earth Sciences* **52**, 1529-1536.
602 Cao, H., Vervoort, J., Wang, D., Li, G. & Neill, O. 2016. Triassic monazite ages and its geological significance of
603 garnet-mica schist in Fenzishan Group, Jiaobei Massif. *Acta Petrologica Sinica* **32**, 3800-3816 In Chinese with
604 English abstract.
605 Cao, Y., Zhou, X. & Liu, J. 2022. Discovery of high pressure granulite in the Daqu Island, East China Sea and its
606 tectonic implications. *Journal of Jilin University Earth Science Edition*, doi: 10.13278/j.cnki.jjuese.20210343 In
607 Chinese with English abstract.
608 Carter, A. & Clift, P. D. 2008. Was the Indosinian orogeny a Triassic mountain building or a thermotectonic
609 reactivation event? *Comptes Rendus Geoscience* **340**, 83-93.
610 Carter, A., Roques, D., Bristow, C. & Kinny, P. 2001. Understanding Mesozoic accretion in Southeast Asia:
611 significance of Triassic thermotectonism Indosinian orogeny in Vietnam. *Geology* **29**, 211.
612 Cawood, P. A., Wang, W., Zhao, T., Xu, Y., Mulder, J. A., Pisarevsky, S. A., Zhang, L., Gan, C., He, H., Liu, H., Qi,
613 L., Wang, Y., Yao, J., Zhao, G., Zhou, M.-F. & Zi, J.-W. 2020. Deconstructing South China and consequences for
614 reconstructing Nuna and Rodinia. *Earth-Science Reviews* **204**.
615 Cawood, P. A., Zhao, G., Yao, J., Wang, W., Xu, Y. & Wang, Y. 2018. Reconstructing South China in Phanerozoic
616 and Precambrian supercontinents. *Earth-Science Reviews* **186**, 173-194.
617 Chapman, T., Milan, L. A., Metcalfe, I., Blevin, P. L. & Crowley, J. 2022. Pulses in silicic arc magmatism initiate
618 end-Permian climate instability and extinction. *Nature Geoscience* **15**, 411-416.
619 Chen, F., Guo, J. H., Jiang, L. L., Siebel, W., Cong, B. & Satir, M. 2003. Provenance of the Beihuaiyang lower-grade
620 metamorphic zone of the Dabie ultrahigh-pressure collisional orogen, China: evidence from zircon ages. *Journal*
621 *of Asian Earth Sciences* **22**, 343-352.
622 Chu, Y., Faure, M., Lin, W., Wang, Q. & Ji, W. 2012. Tectonics of the Middle Triassic intracontinental Xuefengshan
623 Belt, South China: new insights from structural and chronological constraints on the basal décollement zone.
624 *International Journal of Earth Sciences* **101**, 2125-2150.
625 Clarkson, M. O., Kasemann, S. A., Wood, R. A., Lenton, T. M., Daines, S. J., Richoz, S., Ohnemueller, F., Meixner,
626 A., Poulton, S. W. & Tipper, E. T. 2015. Ocean acidification and the Permo-Triassic mass extinction. *Science* **348**,
627 229-232.
628 Cocks, L. R. M. & Torsvik, T. H. 2013. The dynamic evolution of the Palaeozoic geography of eastern Asia. *Earth-*
629 *Science Reviews* **117**, 40-79.
630 Cui, X., Wang, J., Wang, X.-C., Wilde, S. A., Ren, G., Li, S., Deng, Q., Ren, F. & Liu, J. 2021. Early crustal
631 evolution of the Yangtze Block: Constraints from zircon U-Pb-Hf isotope systematics of 3.1–1.9 Ga granitoids in
632 the Cuoke Complex, SW China. *Precambrian Research* **357**.
633 Davydov, V. I. & Karasev, E. V. 2021. The Influence of the Permian-Triassic Magmatism in the Tunguska Basin,
634 Siberia on the Regional Floristic Biota of the Permian-Triassic Transition in the Region. *Frontiers in Earth*
635 *Science* **9**.
636 Dong, Y., Yang, Z., Liu, X., Sun, S., Li, W., Cheng, B., Zhang, F., Zhang, X., He, D. & Zhang, G. 2016. Mesozoic
637 intracontinental orogeny in the Qinling Mountains, central China. *Gondwana Research* **30**, 144-158.
638 Dong, Y., Zhang, G., Neubauer, F., Liu, X., Genser, J. & Hauzenberger, C. 2011. Tectonic evolution of the Qinling
639 orogen, China: Review and synthesis. *Journal of Asian Earth Sciences* **41**, 213-237.
640 Erwin, D. H. 1990. The end permian mass extinction. *Annu. Rev. Ecol. Syst* **21**, 69-91.
641 Erwin, D. H., Bowring, S. A. & Yugan, J. 2002. End-Permian mass extinction: a review. In: Koeberl, C. &
642 MacLeod, K. G. eds. *Catastrophic events and mass extinction: impacts and beyond*. Boulder, Colorado:
643 Geological Society of America Special Paper, 363-383.
644 Fan, J.-X., Shen, S.-Z., Erwin, D. H., Sadler, P. M., MacLeod, N., Cheng, Q.-M., Hou, X.-D., Yang, J., Wang, X.-d.,
645 Wang, Y., Zhang, H., Chen, X., Li, G.-x., Shi, Y.-c., Yuan, D.-x., Chen, Q., Zhang, L.-n., Li, C. & Zhao, Y.-y.
646 2020. A high-resolution summary of Cambrian to Early Triassic marine invertebrate biodiversity. *Science* **367**,
647 272-277.

Faure, M., Lepvrier, C., Nguyen, V. V., Vu, T. V., Lin, W. & Chen, Z. 2014. The South China block-Indochina collision: Where, when, and how? *Journal of Asian Earth Sciences* **79**, 260-274.

Faure, M., Lin, W., Chu, Y. & Lepvrier, C. 2016. Triassic tectonics of the Ailaoshan Belt SW China: Early Triassic collision between the South China and Indochina Blocks, and Middle Triassic intracontinental shearing. *Tectonophysics* **683**, 27-42.

Gilder, S. A., Leloup, P. H., Courtillot, V., Chen, Y., Coe, R. S., Zhao, X., Xiao, W., Halim, N., Cogné, J.-P. & Zhu, R. 1999. Tectonic evolution of the Tancheng-Lujiang Tan-Lu fault via Middle Triassic to Early Cenozoic paleomagnetic data. *Journal of Geophysical Research: Solid Earth* **104**, 15365-15390.

Gupta, S., Rodgers, J., Hsü, K. J., Shu, S., Jiliang, L., Haihong, C., Haipo, P. & Sengor, A. 1989. Comments and Reply on" Mesozoic overthrust tectonics in south China". *Geology* **17**, 669-673.

Hsü, K. J., Sun, S., Li, J., Chen, H., Pen, H. & Sengor, A. 1988. Mesozoic overthrust tectonics in south China. *Geology* **16**, 418-421.

Huang, B., Yan, Y., Piper, J. D. A., Zhang, D., Yi, Z., Yu, S. & Zhou, T. 2018. Paleomagnetic constraints on the paleogeography of the East Asian blocks during Late Paleozoic and Early Mesozoic times. *Earth-Science Reviews* **186**, 8-36.

Huang, J. 1960. Preliminary summarization of geologic tectonics in China. *Acta Geologica Sinica in Chinese* **40**, 1-37.

Huyskens, M.H., Yin, Q.Z., Li, Q.L., Li, X.H., Liu, Y., Tang, G.Q., 2016, In Search of New Monazite and Titanite Standard Minerals for In Situ U-Pb Geochronology. *47th Lunar and Planetary Science Conference*.

Isozaki, Y. 1997. Permo-Triassic Boundary Superanoxia and Stratified Superocean: records from lost deep sea. *Science* **276**, 235-238.

Jahn, B. m., Liu, D., Wan, Y., Song, B. & Wu, J. 2008. Archean crustal evolution of the Jiaodong Peninsula, China, as revealed by zircon SHRIMP geochronology, elemental and Nd-isotope geochemistry. *American Journal of Science* **308**, 232-269.

Jian, P., Kröner, A. & Zhou, G. 2012. SHRIMP zircon U–Pb ages and REE partition for high-grade metamorphic rocks in the North Dabie complex: Insight into crustal evolution with respect to Triassic UHP metamorphism in east-central China. *Chemical Geology* **328**, 49-69.

Jiang, Y., Xing, G., Yuan, Q., Zhao, X., Duan, Z. & Dong, X. 2016. The first discovery of Permian metamorphic rocks in Zhoushan Islands, Zhejiang Province. *Geological Bulletin of China* **35**, 1046-1055 In Chinese with English abstract.

Jin, Y. G., Wang, Y., Wang, W., Shang, Q. H., Cao, C. Q. & Erwin, D. H. 2000. Pattern of Marine Mass Extinction Near the Permian-Triassic boundary in South China. *Science* **289**, 432-436.

Lepvrier, C., Maluski, H., Van Tich, V., Leyreloup, A., Truong Thi, P. & Van Vuong, N. 2004. The Early Triassic Indosinian orogeny in Vietnam Truong Son Belt and Kontum Massif; implications for the geodynamic evolution of Indochina. *Tectonophysics* **393**, 87-118.

Li, J., Dong, S., Zhang, Y., Zhao, G., Johnston, S. T., Cui, J. & Xin, Y. 2016. New insights into Phanerozoic tectonics of south China: Part 1, polyphase deformation in the Jiuling and Lianyunshan domains of the central Jiangnan Orogen. *Journal of Geophysical Research: Solid Earth* **121**, 3048-3080.

Li, J., Zhang, Y., Zhao, G., Johnston, S. T., Dong, S., Koppers, A., Miggins, D. P., Sun, H., Wang, W. & Xin, Y. 2017a. New insights into Phanerozoic tectonics of South China: Early Paleozoic sinistral and Triassic dextral transpression in the east Wuyishan and Chencai domains, NE Cathaysia. *Tectonics* **36**, 819-853.

Li, J., Zhao, G., Johnston, S. T., Dong, S., Zhang, Y., Xin, Y., Wang, W., Sun, H. & Yu, Y. 2017b. Permo-Triassic structural evolution of the Shiwandashan and Youjiang structural belts, South China. *Journal of Structural Geology* **100**, 24-44.

Li, S., Jahn, B.-m., Zhao, S., Dai, L., Li, X., Suo, Y., Guo, L., Wang, Y., Liu, X., Lan, H., Zhou, Z., Zheng, Q. & Wang, P. 2017c. Triassic southeastward subduction of North China Block to South China Block: Insights from new geological, geophysical and geochemical data. *Earth-Science Reviews* **166**, 270-285.

Li, X., Liu, Y., Li, Q., Guo, C., and Chamberlain, K. R., 2009, Precise determination of Phanerozoic zircon Pb/Pb age by multicollector SIMS without external standardization. *Geochemistry Geophysics Geosystems* 10, 4, n/a-n/a.

Li, Q., Wu, F., Li, X., Qiu, Z., Liu, Y., Yang, Y., and Tang, G., 2011, Precisely dating Paleozoic kimberlites in the North China Craton and Hf isotopic constraints on the evolution of the subcontinental lithospheric mantle. *Lithos* 126, 127-134.

Li Q., Yang Y., Shi Y., Lin W., 2013a. Eclogite rutile U-Pb dating: constrant for formation and evolution of continental collisional orogen. *Chinese Science Bulletin* 58, 2279–2284, doi: 10.1360/972013-590.

Li, X., Tang, G., Gong, B., Yang, Y., Hou, K. J., Hu, Z., Li, Q., Liu, Y., and Li, W., 2013b. Qinghu zircon: A working reference for microbeam analysis of U-Pb age and Hf and O isotopes. *Chinese Science Bulletin* 58, 4647-4654.

Li, X. H., Li, W. X., Li, Z. X., Lo, C. H., Wang, J., Ye, M. F. & Yang, Y. H. 2009. Amalgamation between the Yangtze and Cathaysia Blocks in South China: Constraints from SHRIMP U–Pb zircon ages, geochemistry and Nd–Hf isotopes of the Shuangxiwu volcanic rocks. *Precambrian Research* **174**, 117-128.

Li, X. H., Li, Z. X., Li, W. X. & Wang, Y. 2006. Initiation of the Indosinian orogeny in South China: Evidence for a Permian magmatic arc on Hainan Island. *The Journal of Geology* **114**, 341-353.

Li, Z.-X. 1994. Collision between the North and South China blocks: a crustal-detachment model for suturing in the region east of the Tanlu fault. *Geology* **22**, 739-742.

Li, X.-H., Li, Z.-X., He, B., Li, W.-X., Li, Q.-L., Gao, Y. & Wang, X.-C. 2012a. The Early Permian active continental margin and crustal growth of the Cathaysia Block: In situ U–Pb, Lu–Hf and O isotope analyses of detrital zircons. *Chemical Geology* **328**, 195-207.

Li, Z.-X., Li, X.-H., Chung, S.-L., Lo, C.-H., Xu, X. & Li, W.-X. 2012b. Magmatic switch-on and switch-off along the South China continental margin since the Permian: Transition from an Andean-type to a Western Pacific-type plate boundary. *Tectonophysics* **532-535**, 271-290.

Li, Z. X. & Li, X. H. 2007. Formation of the 1300-km-wide intracontinental orogen and postorogenic magmatic province in Mesozoic South China: A flat-slab subduction model. *Geology* **35**, 179-182.

Li, Z. X., Mitchell, R. N., Spencer, C. J., Ernst, R., Pisarevsky, S., Kirscher, U. & Murphy, J. B. 2019. Decoding Earth's rhythms: Modulation of supercontinent cycles by longer superocean episodes. *Precambrian Research* **323**, 1-5.

Lin, S., Xing, G., Davis, D. W., Yin, C., Wu, M., Li, L., Jiang, Y. & Chen, Z. 2018. Appalachian-style multi-terrane Wilson cycle model for the assembly of South China. *Geology* **46**, 319-322.

Lin, W., Monié, P., Faure, M., Schärer, U., Shi, Y., Breton, N. L. & Wang, Q. 2011. Cooling paths of the NE China crust during the Mesozoic extensional tectonics: Example from the south-Liaodong peninsula metamorphic core complex. *Journal of Asian Earth Sciences* **42**, 1048-1065.

Liu, F., Liu, P., Wang, F., Liu, J., Meng, E., Cai, J. & Shi, J. 2014. U–Pb dating of zircons from granitic leucosomes in migmatites of the Jiaobei Terrane, southwestern Jiao–Liao–Ji Belt, North China Craton: Constraints on the timing and nature of partial melting. *Precambrian Research* **245**, 80-99.

Liu, F. L., Gerdes, A., Liou, J. G., Xue, H. M. & Liang, F. H. 2006. SHRIMP U-Pb zircon dating from Sulu-Dabie dolomitic marble, eastern China: constraints on prograde, ultrahigh-pressure and retrograde metamorphic ages. *Journal of Metamorphic Geology* **24**, 569-589.

Liu, L., Liu, F., Guo, J., Liu, P., Wang, W. & Cai, J. 2021. Geochronological and geochemical constraints on the non-ultrahigh-pressure metasedimentary blocks of North China affinity within the Sulu ultrahigh-pressure belt, eastern China, and tectonic implications. *International Geology Review*, DOI: 10.1080/00206814.00202021.01882889.

Liu, L., Liu, F., Santosh, M., Wang, H. & Ji, L. 2018. Paleoproterozoic and Triassic metamorphic events in the Jiaobei Terrane, Jiao-Liao-Ji Belt, China: Hidden clues on multiple metamorphism and new insights into complex tectonic evolution. *Gondwana Research* **60**, 105-128.

Liu, P., Liu, F., Yang, H., Wang, F. & Liu, J. 2012. Protolith ages and timing of peak and retrograde metamorphism of the high-pressure granulites in the Shandong Peninsula, eastern North China Craton. *Geoscience Frontiers* **3**, 923-943.

Liu, X. C., Jahn, B. M., Hu, J., Li, S. Z., Liu, X. & Song, B. 2011. Metamorphic patterns and SHRIMP zircon ages of medium-to-high grade rocks from the Tongbai orogen, central China: implications for multiple accretion/collision processes prior to terminal continental collision. *Journal of Metamorphic Geology* **29**, 979-1002.

Mao, J., Ye, H., Liu, K., Li, Z., Takahashi, Y., Zhao, X. & Kee, W.-S. 2013. The Indosinian collision–extension event between the South China Block and the Palaeo-Pacific plate: Evidence from Indosinian alkaline granitic rocks in Dashuang, eastern Zhejiang, South China. *Lithos* **172-173**, 81-97.

Meng, L. & Lin, W. 2021. Late Triassic contractional tectonics in the overriding plate of the Sulu orogenic belt, Eastern China. *Tectonophysics* **806**, DOI: 10.1016/j.tecto.2021.228793.

Meng, Q. R. & Zhang, G. W. 1999. Timing of collision of the North and South China blocks: Controversy and reconciliation. *Geology* **27**, 123-126.

Metcalfe, I. 1998. Palaeozoic and Mesozoic geological evolution of the SE Asian region: multidisciplinary constraints and implications for biogeography. *Biogeography and Geological Evolution of SE Asian*, 25-41.

Metcalfe, I. 2006. Palaeozoic and Mesozoic tectonic evolution and palaeogeography of East Asian crustal fragments: The Korean Peninsula in context. *Gondwana Research* **9**, 24-46.

759 Metcalfe, I. 2013. Gondwana dispersion and Asian accretion: Tectonic and palaeogeographic evolution of eastern
760 Tethys. *Journal of Asian Earth Sciences* **66**, 1-33.
761 Meinhold, G. 2010. Rutile and Its Application in Earth Sciences. *Earth-Science Reviews* **102**, 1-28.
762 Nam, T. N., Sano, Y., Terada, K., Toriumi, M., Van Quynh, P. & Dung, L. T. 2001. First SHRIMP U-Pb zircon dating
763 of granulites from the Kontum massif Vietnam and tectonothermal implications. *Journal of Asian Earth Sciences*
764 **19**, 77-84.
765 Oh, C. W. 2015. The Continental Collision Process Deduced from the Metamorphic Pattern in the Dabie-Hongseong
766 and Himalayan Collision Belts. *Subduction Dynamics: From Mantle Flow to Mega Disasters* **211**, 19.
767 Okay, A. I., Xu, S. & Sengor, A. C. 1989. Coesite from the Dabie Shan eclogites, central China. *European Journal of*
768 *Mineralogy* **1**, 595-598.
769 Qiu, Y. M., Gao, S., McNaughton, N. J., Groves, D. I. & Ling, W. 2000. First evidence of> 3.2 Ga continental crust
770 in the Yangtze craton of south China and its implications for Archean crustal evolution and Phanerozoic tectonics.
771 *Geology* **28**, 11-14.
772 Roberts, M. P. & Finger, F. 1997. Do U-Pb zircon ages from granulites reflect peak metamorphic conditions?
773 *Geology* **25**, 319-322.
774 Roger, F., Maluski, H., Leyreloup, A., Lepvrier, C. & Truong Thi, P. 2007. U–Pb dating of high temperature
775 metamorphic episodes in the Kon Tum Massif Vietnam. *Journal of Asian Earth Sciences* **30**, 565-572.
776 Rowley, D. B., Ziegler, A. M., Gyou, N., Hsü, K. J., Shu, S., Jiliang, L., Haihong, C., Haipo, P. & Sengor, A. 1989.
777 Comment and Reply on" Mesozoic overthrust tectonics in south China". *Geology* **17**, 384-387.
778 Schmädicke, E., Will, T. M., Ling, X., Li, X.-H. & Li, Q.-L. 2018. Rare peak and ubiquitous post-peak zircon in
779 eclogite: Constraints for the timing of UHP and HP metamorphism in Erzgebirge, Germany. *Lithos* **322**, 250-267.
780 Scotese, C. 1997. Paleogeographic Atlas, Paleomap progress report 90-0497. *University of Texas at Arlington*.
781 Arlington: http://scotese.com/.
782 Şengör, A. M. C. & Atayman, S. 2009. The Permian extinction and the Tethys: an excercise in global geology. *The*
783 *Geological Society of America, USA*, doi.org/10.1130/SPE1448.
784 Shen, J., Chen, J., Algeo, T. J., Yuan, S., Feng, Q., Yu, J., Zhou, L., O'Connell, B. & Planavsky, N. J. 2019. Evidence
785 for a prolonged Permian-Triassic extinction interval from global marine mercury records. *Nat Commun* **10**, 1563.
786 Shen, L., Yu, J.-H., O'Reilly, S. Y., Griffin, W. L. & Wang, Q. 2016. Widespread Paleoproterozoic basement in the
787 eastern Cathaysia Block: Evidence from metasedimentary rocks of the Pingtan–Dongshan metamorphic belt, in
788 southeastern China. *Precambrian Research* **285**, 91-108.
789 Shen, Y., Farquhar, J., Zhang, H., Masterson, A., Zhang, T. & Wing, B. A. 2011. Multiple S-isotopic evidence for
790 episodic shoaling of anoxic water during Late Permian mass extinction. *Nat Commun* **2**, 210.
791 Shu, L., Faure, M., Wang, B., Zhou, X. & Song, B. 2008. Late Palaeozoic-Early Mesozoic geological features of
792 south China: Response to the Indosinian collision events in southeast Asia. *Comptes Rendus Geosciences* **340**,
793 151-165.
794 Shu, L. S., Jahn, B. M., Charvet, J., Santosh, M., Wang, B., Xu, X. S. & Jiang, S. Y. 2014. Early Paleozoic
795 depositional environment and intraplate tectono-magmatism in the Cathaysia Block South China: Evidence from
796 stratigraphic, structural, geochemical and geochronological investigations. *American Journal of Science* **314**, 154-
797 186.
798 Sláma, J., Košler, J., Condon, D. J., Crowley, J. L., Gerdes, A., Hanchar, J. M., Horstwood, M. S. A., Morris, G. A.,
799 Nasdala, L., Norberg, N., Schaltegger, U., Schoene, B., Tubrett, M. N., and Whitehouse, M. J., 2008. Plešovice
800 zircon — A new natural reference material for U–Pb and Hf isotopic microanalysis. *Chemical Geology* 249, 1-
801 35.
802 Song, M., Shu, L., Santosh, M. & Li, J. 2015. Late Early Paleozoic and Early Mesozoic intracontinental orogeny in
803 the South China Craton: Geochronological and geochemical evidence. *Lithos* **232**, 360-374.
804 Spencer, K. J., Hacker, B. R., Kylander-Clark, A. R. C., Andersen, T. B., Cottle, J. M., Stearns, M. A., Poletti, J. E.,
805 and Seward, G. G. E., 2013. Campaign-style titanite U–Pb dating by laser-ablation ICP: Implications for crustal
806 flow, phase transformations and titanite closure. *Chemical Geology* 341, 84-101.
807 Stampfli, G. M., Hochard, C., Vérard, C., Wilhem, C. & vonRaumer, J. 2013. The formation of Pangea.
808 *Tectonophysics* **593**, 1-19.
809 Torsvik, T. H. & Cocks, R. M. 2016. Earth history and Paleogeography. *Cambridge Universty Press*,
810 doi.org/10.1017/9781316225523.
811 Viglietti, P. A., Benson, R. B. J., Smith, R. M. H., Botha, J., Kammerer, C. F., Skosan, Z., Butler, E., Crean, A.,
812 Eloff, B., Kaal, S., Mohoi, J., Molehe, W., Mtalana, N., Mtungata, S., Ntheri, N., Ntsala, T., Nyaphuli, J., October,
813 P., Skinner, G., Strong, M., Stummer, H., Wolvaardt, F. P. & Angielczyk, K. D. 2021. Evidence from South Africa
814 for a protracted end-Permian extinction on land. *Proc Natl Acad Sci U S A* **118**.

Wang, L., Kusky, T. M., Polat, A., Wang, S., Jiang, X., Zong, K., Wang, J., Deng, H. & Fu, J. 2014. Partial melting of deeply subducted eclogite from the Sulu orogen in China. *Nat Commun* **5**, 5604.

Wang, W., Zhou, M.-F., Yan, D.-P., Li, L. & Malpas, J. 2013a. Detrital zircon record of Neoproterozoic active-margin sedimentation in the eastern Jiangnan Orogen, South China. *Precambrian Research* **235**, 1-19.

Wang, X. & Liou, J. 1991. Regional ultrahigh-pressure coesite-bearing eclogitic terrane in central China: Evidence from country rocks, gneiss, marble, and metapelite. *Geology* **19**, 933-936.

Wang, X., Liou, J. & Mao, H. 1989. Coesite-bearing eclogite from the Dabie Mountains in central China. *Geology* **17**, 1085-1088.

Wang, Y.-F., Li, X.-H., Jin, W. & Zhang, J.-H. 2015. Eoarchean ultra-depleted mantle domains inferred from ca. 3.81Ga Anshan trondhjemitic gneisses, North China Craton. *Precambrian Research* **263**, 88-107.

Wang, Y., Fan, W., Zhang, G. & Zhang, Y. 2013b. Phanerozoic tectonics of the South China Block: Key observations and controversies. *Gondwana Research* **23**, 1273-1305.

Wang, Y., Wang, Y., Zhang, Y., Cawood, P. A., Qian, X., Gan, C., Zhang, F. & Zhang, P. 2021. Triassic two-stage intra-continental orogensis of the South China Block, driven by Paleotethyan closure and interactions with adjoining blocks. *Journal of Asian Earth Sciences* **206**.

Wang, Y., Wu, C., Zhang, A., Fan, W., Zhang, Y., Zhang, Y., Peng, T. & Yin, C. 2012. Kwangsian and Indosinian reworking of the eastern South China Block: Constraints on zircon U–Pb geochronology and metamorphism of amphibolites and granulites. *Lithos* **150**, 227-242.

Wang, Z., Deng, Q., Duan, T., Yang, F., Du, Q., Xiong, X., Liu, H. & Cao, B. 2018. 2.85 Ga and 2.73 Ga A-type granites and 2.75 Ga trondhjemite from the Zhongxiang Terrain: Implications for early crustal evolution of the Yangtze Craton, South China. *Gondwana Research* **61**, 1-19.

Williams, I.S., 1998. U-Th-Pb geochronology by ion microprobe. In: Mckibben, M.A., Shanks, W.C., Ridley, W.I. Eds, Applications of Mrcoanalytical Techniques to Understanding Mineralizing Processes 7. *Rev. Geol.* 1-35.

Winguth, C. & Winguth, A. M. E. 2012. Simulating Permian–Triassic oceanic anoxia distribution: Implications for species extinction and recovery. *Geology* **40**, 127-130.

Wu, F.-Y., Yang, J.-H., Xu, Y.-G., Wilde, S. A. & Walker, R. J. 2019. Destruction of the North China Craton in the Mesozoic. *Annual Review of Earth and Planetary Sciences* **47**, 173-195.

Wu, F. Y., Wan, B., Zhao, L., Xiao, W. J. & Zhu, R. X. 2020. Tethyan geodynamics. *Acta Petrologica Sinica* **36**, 1627-1674 In Chinese with English abstract.

Wu, M., Zhao, G., Sun, M., Li, S., Bao, Z., Tam, P. Y., Eizenhöefer, P. R. & He, Y. 2014. Zircon U–Pb geochronology and Hf isotopes of major lithologies from the Jiaodong Terrane: Implications for the crustal evolution of the Eastern Block of the North China Craton. *Lithos* **190-191**, 71-84.

Wu, S., Karius, V., Schmidt, B. C., Simon, K., and Worner, G., 2018, Comparison of Ultrafine Powder Pellet and Flux-free Fusion Glass for Bulk Analysis of Granitoids by Laser Ablation-Inductively Coupled Plasma-Mass Spectrometry. *Geostandards and Geoanalytical Research* 42, 575-591.

Wu, Y.-B. & Zheng, Y.-F. 2013. Tectonic evolution of a composite collision orogen: An overview on the Qinling–Tongbai–Hong'an–Dabie–Sulu orogenic belt in central China. *Gondwana Research* **23**, 1402-1428.

Wu, Y. 2009. Multistage evolution of continental collision orogen: A case study for western Dabie orogen. *Chinese Science Bulletin* **54**, 2568-2579.

Wu, Y. B., Zheng, Y. F., Tang, J., Gong, B., Zhao, Z. F. & Liu, X. 2007. Zircon U-Pb dating of water-rock interaction during Neoproterozoic rift magmatism in South China. *Chemical Geology* **246**, 65-86.

Xia, Y. & Xu, X. 2019. A Fragment of Columbia Supercontinent: Insight for Cathaysia Block Basement From Tectono-Magmatic Evolution and Mantle Heterogeneity. *Geophysical Research Letters* **46**, 2012-2024.

Xia, Y. & Xu, X. 2020. The epilogue of Paleo-Tethyan tectonics in the South China Block: Insights from the Triassic aluminous A-type granitic and bimodal magmatism. *Journal of Asian Earth Sciences* **190**.

Xiao, W. & He, H. 2005. Early Mesozoic thrust tectonics of the northwest Zhejiang region Southeast China. *Geological Society of America Bulletin* **117**, 945-961.

Xu, S., AI, O., Ji, S., AMC, S., Su, W., Liu, Y. & Jiang, L. 1992. Diamond from the Dabie Shan metamorphic rocks and its implication for tectonic setting. *Science* **256**, 80-82.

Yang, J.-H., Wu, F.-Y., Wilde, S. A., Belousova, E. & Griffin, W. L. 2008. Mesozoic decratonization of the North China block. *Geology* **36**, 467-470.

Ye, H., Wu, C.-Z., Yang, T., Santosh, M., Yao, X.-Z., Gao, B.-F., Wang, X.-L. & Li, W. 2017. Updating the Geologic Barcodes for South China: Discovery of Late Archean Banded Iron Formations in the Yangtze Craton. *Scientific Reports* **7**.

Ye, K., Cong, B. & Ye, D. 2000. The possible subduction of continental material to depths greater than 200km. *Nature* **407**, 734-736.

Yin, A. & Nie, S. 1993. An indentation model for the North and South China collision and the development of the Tan-Lu and Honam fault systems, eastern Asia. *Tectonics* **12**, 801-813.

Yin, H., Jiang, H., Xia, W., Feng, Q., Zhang, N. & Shen, J. 2014. The end-Permian regression in South China and its implication on mass extinction. *Earth-Science Reviews* **137**, 19-33.

Yin, H., Xie, S., Luo, G., Algeo, T. J. & Zhang, K. 2012. Two episodes of environmental change at the Permian–Triassic boundary of the GSSP section Meishan. *Earth-Science Reviews* **115**, 163-172.

Yu, J., Zhou, X., O'Reilly, Y., Zhao, L., Griffin, W., Wang, R., Wang, L. & Chen, X. 2005. Formation history and protolith characteristics of granulite facies metamorphic rock in Central Cathaysia deduced from U-Pb and Lu-Hf isotopic studies of single zircon grains. *Chinese Science Bulletin* **50**, 2080-2089.

Yu, J., Zhou, X., Zhao, L. & Chen, X. 2003. Discovery and implications of granulite facies metamorphic rocks in the eastern Nanling, China. *Acta Petrologica Sinica* **19**, 461-467 In Chinese with English abstract.

Zhai, M. 2011. Cratonization and the Ancient North China Continent: A summary and review. *Science China Earth Sciences* **54**, 1110-1120.

Zhai, M. 2014. Multi-stage crustal growth and cratonization of the North China Craton. *Geoscience Frontiers* **5**, 457-469.

Zhang, A., Ma, L., Liu, H., Cai, Y., Chen, M. & Fang, Q. 2021a. Identification of two-phased late Paleoproterozoic magmatism in the Wuyishan Domain SE China: Implications for the tectonic evolution of the Cathaysia Block. *Precambrian Research* **355**, 106093.

Zhang, G., Guo, A., Wang, Y., Li, S., Dong, Y., Liu, S., He, D., Cheng, S., Lu, R. & Yao, A. 2013a. Tectonics of South China continent and its implications. *Science China Earth Sciences* **56**, 1804-1828.

Zhang, G. W., Cheng, S. Y., Guo, A., Dong, Y. P., Lai, S. & Yao, Y. P. 2004. Mianlue paleo-suture on the southern margin of the Central Orogenic System in Qinling-Dabie - with a discussion of th assembly of the main part of the continent China. *Geological Bulletin of China* **23**, 846-853 In Chinese with English abstract.

Zhang, H., Zhang, F., Chen, J.-B., Erwin, D. H., Syverson, D. D., Ni, P., Rampino, M., Chi, Z., Cai, Y.-f., Xiang, L., Li, W.-Q., Liu, S.-A., Wang, R.-C., Wang, X.-d., Feng, Z., Li, H.-m., Zhang, T., Cai, H.-m., Zheng, W., Cui, Y., Zhu, X.-k., Hou, Z.-q., Wu, F.-y., Xu, Y.-g., Planavsky, N. & Shen, S.-z. 2021b. Felsic volcanism as a factor driving the end-Permian mass extinction. *Science Advances* **7**, eabh1390.

Zhang, J., Qu, J., Zhang, B., Zhao, H., Wang, Y. & Lu, M. 2017. Paleozoic to Mesozoic deformation of eastern Cathaysia: A case study of the Chencai complex, Zhejiang Province, eastern China, and its tectonic implications. *GSA Bulletin*, https://doi.org/10.1130/B31680.31681.

Zhang, R., Lo, C., Chung, S., Grove, M., Omori, S., Iizuka, T., Liou, J. & Tri, T. V. 2013b. Origin and tectonic implication of Ophiolite and eclogite in the Song Ma Suture Zone between the South China and Indochina Block. *Journal of Metamorphic Geology* **31**.

Zhang, R. Y., Lo, C., Li, X. H., Chung, S., Anh, T. T. & Tri, T. V. 2014a. U-Pb dating and tectonic implication of ophiolite and metabasite from the Song Ma Suture zone, Northern Vietnam. *American Journal of Science* **314**.

Zhang, S.-B., Zheng, Y.-F., Wu, Y.-B., Zhao, Z.-F., Gao, S. & Wu, F.-Y. 2006. Zircon isotope evidence for ≥3.5Ga continental crust in the Yangtze craton of China. *Precambrian Research* **146**, 16-34.

Zhang, S.-H., Zhao, Y., Davis, G. A., Ye, H. & Wu, F. 2014b. Temporal and spatial variations of Mesozoic magmatism and deformation in the North China Craton: Implications for lithospheric thinning and decratonization. *Earth-Science Reviews* **131**, 49-87.

Zhao, G. & Zhai, M. 2013. Lithotectonic elements of Precambrian basement in the North China Craton: Review and tectonic implications. *Gondwana Research* **23**, 1207-1240.

Zhao, L., Li, T., Peng, P., Guo, J., Wang, W., Wang, H., Santosh, M. & Zhai, M. 2015a. Anatomy of zircon growth in high pressure granulites: SIMS U–Pb geochronology and Lu–Hf isotopes from the Jiaobei Terrane, eastern North China Craton. *Gondwana Research* **28**, 1373-1390.

Zhao, L., Zhai, M., Santosh, M. & Zhou, X. 2017. Early Mesozoic retrograded eclogite and mafic granulite from the Badu Complex of the Cathaysia Block, South China: Petrology and tectonic implications. *Gondwana Research* **42**, 84-103.

Zhao, L., Zhai, M. & Zhou, X. 2022. Formation of an intracontinental orogen above the Permo-Triassic mantle convection cell in the Paleo-Tethys tectonic realm due to far-field stress derived from continental margins. *Frontiers in Earth Science*, DOI: 10.3389/feart.2022.892787.

Zhao, L., Zhai, M., Zhou, X., Santosh, M. & Ma, X. 2016. Thermal gradient and geochronology of a Paleozoic high-grade terrane in the northeastern Cathaysia block, South China. *Tectonophysics* **691**, 311-327.

Zhao, L., Zhou, X., Zhai, M., Liu, B. & Cui, X. 2018. Petrologic and zircon U–Pb geochronological characteristics of the pelitic granulites from the Badu Complex of the Cathaysia Block, South China. *Journal of Asian Earth Sciences* **158**, 65-79.

927 Zhao, L., Zhou, X., Zhai, M., Santosh, M. & Geng, Y. 2015b. Zircon U–Th–Pb–Hf isotopes of the basement rocks in
928 northeastern Cathaysia block, South China: Implications for Phanerozoic multiple metamorphic reworking of a
929 Paleoproterozoic terrane. *Gondwana Research* **28**, 246-261.
930 Zheng, Y. F., Zhou, J. B., Wu, Y. B. & Xie, Z. 2005. Low-grade metamorphic rocks in the Dabie-Sulu Orogenic Belt:
931 a passive-margin accretionary wedge deformed during continent subduction. *International Geology Review* **47**,
932 851-871.
933 Zhou, L.-G., Xia, Q.-X., Zheng, Y.-F. & Chen, R.-X. 2011. Multistage growth of garnet in ultrahigh-pressure
934 eclogite during continental collision in the Dabie orogen: Constrained by trace elements and U–Pb ages. *Lithos*
935 **127**, 101-127.
936 Zhou, L.-G., Xia, Q.-X., Zheng, Y.-F., Chen, R.-X., Hu, Z. & Yang, Y. 2015. Tectonic evolution from oceanic
937 subduction to continental collision during the closure of Paleotethyan ocean: Geochronological and geochemical
938 constraints from metamorphic rocks in the Hong'an orogen. *Gondwana Research* **28**, 348-370.
939 Zhu, G., Chen, Y., Jiang, D. & Lin, S. 2015. Rapid change from compression to extension in the North China Craton
940 during the Early Cretaceous: Evidence from the Yunmengshan metamorphic core complex. *Tectonophysics* **656**,
941 91-110.
942 Zhu, R.-X., Yang, J.-H. & Wu, F.-Y. 2012. Timing of destruction of the North China Craton. *Lithos* **149**, 51-60.
943
944